


## RESEARCH ARTICLE

# Characteristics and sources of fluorescent aerosols in the central Arctic Ocean

Ivo Beck<sup>1,\*</sup> , Alireza Moallemi<sup>1</sup>, Benjamin Heutte<sup>1</sup>, Jakob Boyd Pernov<sup>1</sup>, Nora Bergner<sup>1</sup>, Margarida Rolo<sup>1</sup>, Lauriane L. J. Quéléver<sup>2</sup>, Tiia Laurila<sup>2</sup>, Matthew Boyer<sup>2</sup>, Tuija Jokinen<sup>2,3</sup>, H el ene Angot<sup>1,4</sup>, Clara J. M. Hoppe<sup>5</sup>, Oliver M uller<sup>6</sup>, Jessie Creamean<sup>7</sup>, Markus M. Frey<sup>8</sup>, Gabriel Freitas<sup>9,10</sup>, Julika Zinke<sup>9,10</sup>, Matt Salter<sup>9,10</sup>, Paul Zieger<sup>9,10</sup>, Jessica A. Mirrielees<sup>11</sup>, Hailey E. Kempf<sup>11</sup>, Andrew P. Ault<sup>11</sup>, Kerri A. Pratt<sup>11,12</sup>, Martin Gysel-Beer<sup>13</sup>, Silvia Henning<sup>14</sup>, Christian Tatzelt<sup>14</sup>, and Julia Schmale<sup>1,\*</sup>

The Arctic is sensitive to cloud radiative forcing. Due to the limited number of aerosols present throughout much of the year, cloud formation is susceptible to the presence of cloud condensation nuclei and ice nucleating particles (INPs). Primary biological aerosol particles (PBAP) contribute to INPs and can impact cloud phase, lifetime, and radiative properties. We present yearlong observations of hyperfluorescent aerosols (HFA), tracers for PBAP, conducted with a Wideband Integrated Bioaerosol Sensor, New Electronics Option during the Multidisciplinary drifting Observatory for the Study of Arctic Climate (MOSAIC) expedition (October 2019–September 2020) in the central Arctic. We investigate the influence of potential anthropogenic and natural sources on the characteristics of the HFA and relate our measurements to INP observations during MOSAIC. Anthropogenic sources influenced HFA during the Arctic haze period. But surprisingly, we also found sporadic “bursts” of HFA with the characteristics of PBAP during this time, albeit with unclear origin. The characteristics of HFA between May and August 2020 and in October 2019 indicate a strong contribution of PBAP to HFA. Notably from May to August, PBAP coincided with the presence of INPs nucleating at elevated temperatures, that is,  $> -9^{\circ}\text{C}$ , suggesting that HFA contributed to the “warm INP” concentration. The air mass residence time and area between May and August and in October were dominated by the open ocean and sea ice, pointing toward PBAP sources from within the Arctic Ocean. As the central Arctic changes drastically due to climate warming with expected implications on aerosol–cloud interactions, we recommend targeted observations of PBAP that reveal their nature (e.g., bacteria, diatoms, fungal spores) in the atmosphere and in relevant surface sources, such as the sea ice, snow on sea ice, melt ponds, leads, and open water, to gain further insights into the relevant source processes and how they might change in the future.

**Keywords:** Arctic, Fluorescent aerosol, Primary biological aerosol particles, MOSAIC expedition, Air-sea-ice-exchange, Ice nucleating particles

<sup>1</sup>Extreme Environments Research Laboratory,  cole Polytechnique F d rale de Lausanne, Sion, Switzerland

<sup>2</sup>Institute for Atmospheric and Earth System Research, University of Helsinki, Helsinki, Finland

<sup>3</sup>Climate & Atmosphere Research Centre (CARE-C), The Cyprus Institute, Nicosia, Cyprus

<sup>4</sup>Universit  Grenoble Alpes, CNRS, INRAE, IRD, Grenoble INP, IGE, Grenoble, France

<sup>5</sup>Marine Biogeosciences, Alfred Wegener Institute—Helmholtz Centre for Polar and Marine Research, Bremerhaven, Germany

<sup>6</sup>Department of Biological Sciences, University of Bergen, Bergen, Norway

<sup>7</sup>Department of Atmospheric Science, Colorado State University, Fort Collins, CO, USA

<sup>8</sup>British Antarctic Survey—Natural Environment Research Council, Cambridge, UK

<sup>9</sup>Department of Environmental Science, Stockholm University, Stockholm, Sweden

<sup>10</sup>Bolin Centre for Climate Research, Stockholm, Sweden

<sup>11</sup>Department of Chemistry, University of Michigan, Ann Arbor, MI, USA

<sup>12</sup>Department of Earth & Environmental Sciences, University of Michigan, Ann Arbor, MI, USA

<sup>13</sup>Laboratory of Atmospheric Chemistry, Paul Scherrer Institute, Villigen PSI, Switzerland

<sup>14</sup>Leibniz Institute for Tropospheric Research, Leipzig, Germany

\*Corresponding authors:

Emails: [julia.schmale@epfl.ch](mailto:julia.schmale@epfl.ch); [ivo.beck@epfl.ch](mailto:ivo.beck@epfl.ch)

## 1. Introduction

The Arctic is experiencing accelerated climate change, warming nearly 4 times faster than the global average—a phenomenon known as Arctic amplification (Serreze and Barry, 2011; Rantanen et al., 2022). Consequently, the Arctic Ocean is witnessing a rapid decline in sea ice and is projected to become practically ice-free for the first time by the middle of this century (Fox-Kemper et al., 2021; Kim et al., 2023). Multiple processes contribute to Arctic amplification, the most prominent being the ice-albedo feedback (Serreze and Barry, 2011). Importantly, clouds also play a crucial role in Arctic amplification. Unlike in lower latitudes, low-level clouds in the Arctic have a greenhouse effect, intensifying warming for most of the year, particularly during winter (Shupe and Intrieri, 2004; Wendisch et al., 2019).

Atmospheric aerosols strongly influence clouds. They impact cloud formation by acting as cloud condensation nuclei (CCN) or ice nucleating particles (INPs), which both alter the lifetimes (Albrecht, 1989) and radiative properties of clouds (Twomey, 1991). The central Arctic cloud regime is dominated by low-level mixed-phase clouds (Morrison et al., 2012). Mixed-phase clouds are particularly influential for the Arctic surface energy budget (Gregory and Morris, 1996; Korolev et al., 2017). Because they have low liquid water amounts, they are very sensitive to changes in the CCN and INP populations (de Boer et al., 2013; Solomon et al., 2018; Eirund et al., 2019). Hence, understanding the availability of both CCN and INPs is critical because their presence and ratio determine the microphysical state of clouds and, thereby, their radiative properties and probability to precipitate (Sotiropoulou et al., 2019). Therefore, aerosols are crucial in shaping the Arctic climate (Serreze and Barry, 2011; Pithan and Mauritsen, 2014).

Despite their significance, atmospheric aerosols and their sources in the high Arctic remain poorly understood (Schmale et al., 2021), leading to high uncertainties in estimating aerosol-driven radiative forcing (Sand et al., 2015; Szopa et al., 2021). Aerosols can originate from anthropogenic and natural sources, possessing complex and diverse characteristics that have distinct impacts on the Arctic climate (Willis et al., 2018; Abbatt et al., 2019). For instance, anthropogenic emissions strongly contribute to the aerosol population during winter and spring through the phenomenon known as Arctic haze. Its annual occurrence involves the transport of air pollution from lower latitudes into the Arctic and contains, among other species, sulfates, particulate organic matter, and black carbon (Stohl, 2006; Quinn et al., 2007). These aerosols accumulate due to less efficient removal processes during this time of year (e.g., Barrie et al., 1981; Stohl, 2006).

Natural aerosols in the high Arctic arise from various sources. Wildfire emissions originating from lower latitudes can be transported to the high Arctic, resulting in elevated black carbon concentrations during spring and summer (Mahmood et al., 2016; Barrett and Sheesley, 2017; Creamean et al., 2018; Winiger et al., 2019). The ocean is another strong contributor to natural aerosols.

In summer, phytoplankton blooms lead to increased dimethyl sulfide production, which undergoes oxidation and produces secondary aerosol (Leck and Persson, 1996; Park et al., 2018; Croft et al., 2019). Moreover, primary sea spray aerosols (SSA) are directly emitted from the sea surface by bursting bubbles, which release film and jet drops (Blanchard, 1989; Leck and Bigg, 2005; de Leeuw et al., 2011). Bubbles are mainly produced in wind-driven whitecaps and breaking waves; however, the formation of nonwind-induced bubbles is also possible (Norris et al., 2011). Leads in the sea ice have also been shown to be a source of locally generated SSA year-round (Scott and Levin, 1972; Nilsson et al., 2001; May et al., 2016; Chen et al., 2022), including sea salt with organic coatings from biological material, like saccharides, amino acids, and fatty acids originating from sea ice algae and bacteria in the sea surface microlayer (SML) (Kirpes et al., 2019). Sea salt aerosols can also be generated by sublimating blowing snow (Huang and Jaeglé, 2017; Frey et al., 2020).

Primary biological aerosol particles (PBAP) are a subset of natural atmospheric aerosols, which are directly emitted into the atmosphere and contain complete or fragmented biological cells, for example, of algae, bacteria, fungal spores, or pollen (Deepak and Vali, 1992; Després et al., 2012; Fröhlich-Nowoisky et al., 2016). PBAP can be efficient INPs (Jayaweera and Flanagan, 1982; Pratt et al., 2009; Kanji et al., 2017; Huang et al., 2021), initiating the formation of ice crystals at temperatures above  $-15^{\circ}\text{C}$  (Pöschl et al., 2010; Hoose and Möhler, 2012). They can also act as a giant CCN, affecting the formation process, lifetime, and optical properties of Arctic mixed-phase clouds (Möhler et al., 2007; Orellana et al., 2011; Solomon et al., 2018). PBAP originate from both marine and terrestrial sources (Després et al., 2012). Various types of PBAP, such as airborne pollen and bacteria, can originate from terrestrial vegetation or can be suspended along with other coarse-mode aerosols, such as dust, and transported to the high Arctic (Campbell et al., 1999; Wéry et al., 2017). The SML contains biogenic organic compounds and microorganisms like bacteria, algae, and viruses that may be emitted with SSA (Leck and Bigg, 1999; Bigg and Leck, 2008; Orellana et al., 2011; Patterson et al., 2016).

Despite the harsh climatic conditions in the central Arctic, several studies have demonstrated the presence of various types of PBAP, including pollen, bacteria, and fungi (e.g., Campbell et al., 1999; Cuthbertson et al., 2017; Malard et al., 2018; Pusz and Urbaniak, 2021). While these studies have provided valuable insights into the diversity and potential sources of Arctic PBAP, they remain limited, and more quantitative measurements are needed to understand better the extent to which PBAP impact the Arctic climate through modulating cloud phase (Burrows et al., 2022). For example, the strength of marine PBAP as a source in the Arctic is hypothesized to potentially increase as retreating sea ice reveals more open water, impacting phytoplankton bloom timing and locations and the abundance of microorganisms in the SML (Wassmann

and Reigstad, 2011; Arrigo and Van Dijken, 2015; Abbatt et al., 2019).

Detecting and studying PBAP poses challenges due to their small fraction in the atmospheric aerosol number concentrations (Fröhlich-Nowoisky et al., 2016). Most Arctic PBAP studies rely on filter sampling with relatively low time resolution and offline analysis. For example, Fu et al. (2015) analyzed weekly collected filter samples from February until June from the Canadian High Arctic at Station Alert to measure the fluorescent properties of water-soluble organic carbon (WSOC). They observed a transition from humic-like to protein-like fluorescent particles from winter to summer and suggested a shift from transported aerosols to more local ones originating from sea-to-air emissions. They also observed increased tracers of fungal spores and pollen toward summer. More recently, Jung et al. (2023) measured the fluorescent properties of WSOC, also collected on filters, simultaneously with marine biological parameters in the Arctic Ocean during the summer of 2016. They found high fluorescence intensities of protein-like components over the sea-ice-covered areas compared to more humic-like components in coastal regions. This indicates increased biological contribution over sea ice. However, such offline measurements offer relatively poor temporal resolution. This limitation makes it difficult to establish associations between observed PBAP and short-term, small-scale meteorological, or environmental variables, hindering a deeper understanding of PBAP sources.

In recent years, the development of new online methods using ultraviolet light-induced fluorescence (UV-LIF) instruments has revolutionized the detection of PBAP (Forde et al., 2019; Moallemi et al., 2021; Freitas et al., 2022). These methods enable real-time measurement of PBAP based on their fluorescence properties (Gabey et al., 2010). UV-LIF methods detect fluorescent particles containing biological fluorophores, such as the amino acids tryptophan, phenylalanine, tyrosine, flavines, and the co-enzyme nicotinamide adenine dinucleotide (NADH) (Savage et al., 2017). However, potential interferences from nonbiological fluorescent aerosols (FA), such as those generated by combustion or the presence of humic-like substances (HULIS), can create challenges in distinguishing PBAP from other FA (Pöhlker et al., 2012). Nonetheless, UV-LIF methods offer valuable insights into the occurrence, processes, and contribution of fluorescent PBAP, thanks to their high temporal resolution.

UV-LIF instruments have been deployed in various studies to estimate PBAP concentrations in polar and remote atmospheric environments. For example, Crawford et al. (2017) measured bio-FA concentrations at Halley VI research station in Antarctica, finding a strong correlation with wind speed. Moallemi et al. (2021) measured FA in the Southern Ocean and associated them with PBAP, SSA, and marine biological activity. Kawana et al. (2024) investigated marine biological indicators and FA, identifying PBAP and correlating them with INP concentrations in the North Pacific, Bering Sea, and Arctic Ocean. They found that marine biology contributed to the sources of PBAP. In

a long-term study in a Finnish boreal forest, Schneider et al. (2021) used UV-LIF aerosol measurements to identify biological particles. They found that specific biological particles, namely, pollen and fungi, served as INPs. In a recent study, Perring et al. (2023) measured FA as a proxy of PBAP from an airplane above the Arctic Ocean in Summer 2017. They found no relationship between PBAP and marine sources at low altitudes and attributed PBAP concentrations to terrestrial sources. Freitas et al. (2023) identified PBAPs using a UV-LIF instrument (multiparameter bioaerosol spectrometer) at Zeppelin station in Ny-Ålesund, Svalbard, and found a relation to proteinaceous INP concentrations at freezing temperatures  $>-15^{\circ}\text{C}$ . They found the highest PBAP concentrations between  $10^{-3}\text{ L}^{-1}$  and  $10^{-1}\text{ L}^{-1}$  in summer.

Here, we report UV-LIF-based observations from the Multidisciplinary drifting Observatory for the Study of Arctic Climate (MOSAIC) expedition that provided an unprecedented opportunity to measure FA in the central Arctic Ocean throughout an entire year. From October 2019 to September 2020, the expedition aimed to study climate-relevant processes in the sea ice, ocean, and atmosphere and their interactions in the central Arctic (Shupe et al., 2022). We present an overview of FA measured by a Wide-band Integrated Bioaerosol Sensor, New Electronics Option (WIBS-NEO, Droplet Measurement Technologies, Longmont, CO, USA), referred to as the WIBS. We describe the sampling methods, data sets, and instrumentation (Section 2). Furthermore, we explore the annual cycle of FA and investigate the factors that influence their characteristics in Section 3.1 and subsections. To better understand their variability, we categorize the data into 3 periods and analyze potential sources, including biological and nonbiological factors, such as Arctic haze, wind-induced aerosolization, and sea spray generation in the subsequent sections. Additionally, we address the challenges associated with studying FA in the Arctic and discuss the potential implications of these measurements in advancing our understanding of aerosol–cloud interactions, specifically in relation to INPs. Lastly, we outline future research directions and emphasize the importance of complementary measurements alongside FA observations in the Arctic.

## 2. Methods

In this study, we utilize data collected during the MOSAIC expedition, which involved the research icebreaker *RV Polarstern* anchoring to an ice floe and drifting across the Arctic Ocean. For more comprehensive information on the expedition, as well as overviews of the atmospheric, oceanic, and ice observations, please refer to Shupe et al. (2022), Rabe et al. (2022), and Nicolaus et al. (2022), respectively.

### 2.1. Drift track

**Figure 1** illustrates the drift track of *RV Polarstern*. The start of the drift is marked with an “o,” and the end is denoted by an “x.” In October 2019, the beginning of the drift, *RV Polarstern* was positioned at  $85^{\circ}\text{N}$ ,  $134^{\circ}\text{E}$ , north of the Laptev Sea and approximately 600 km away from

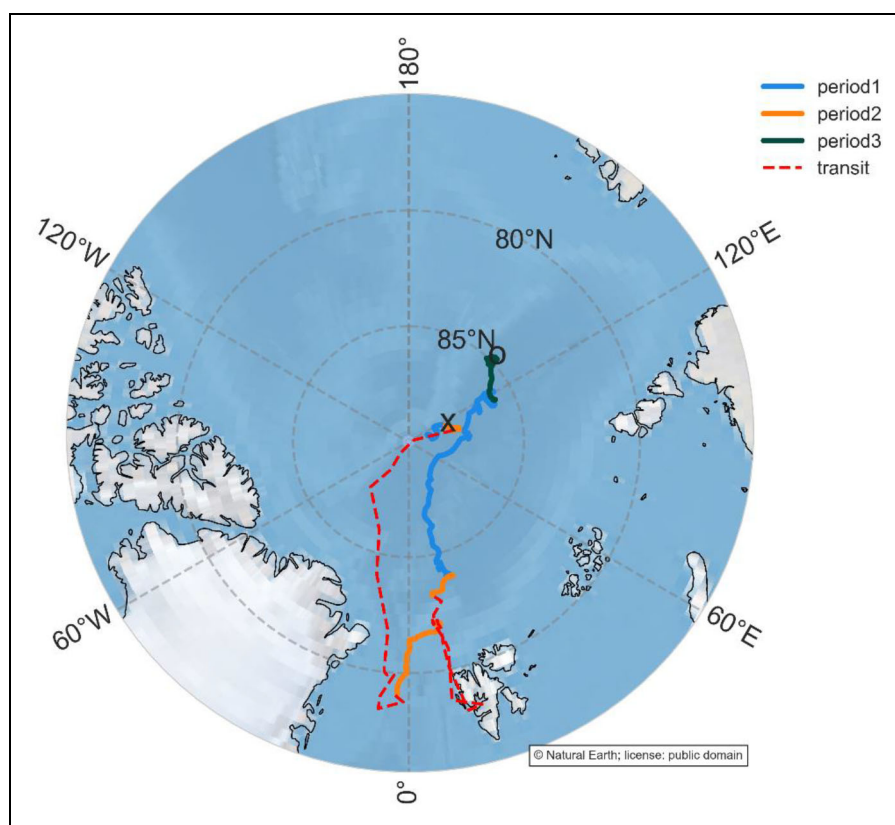


**Figure 1. Drift track of the research vessel *RV Polarstern* during the Multidisciplinary drifting Observatory for the Study of Arctic Climate expedition.** Colors indicate the 3 periods of the drift described in Section 3.1.2. Red dashed lines indicate periods when the ship was in transit, which are excluded from the fluorescent aerosol data analysis. The drift's start (October 4, 2019) and the end (September 20, 2020) are marked with an “o” and an “x,” respectively. Dates of period 1: From November 11, 2019, to April 30, 2020, and from September 1, 2020, to September 20, 2020. Dates of period 2: From May 1, 2020, to August 31, 2020. Dates of Period 3: From April 10, 2019, to November 10, 2019. Dates of transit: May 19, 2020, to June 17, 2020, and August 4, 2020, to August 21, 2020.

Severnaya Zemlya. As the expedition progressed, the ship drifted further northwest and reached 88°N, 56°E in February 2020, before it drifted southwest and approached the ice edge, reaching its southernmost drift position at 79°N, 2°W in the Fram Strait by the end of July 2020. Three periods of the drift are color-coded in **Figure 1**. These periods will be discussed in Section 3.1.2. The drift was interrupted between May 16 and June 18, 2020, when the ship traveled to Svalbard for crew exchange. From July 31 to August 21, 2020, the ship relocated to a new position at 88°N, 104°E to initiate the final phase of the drift, which concluded on September 20, 2020, at 89°N, 110°E. The position of the *RV Polarstern* was tracked using a position sensor on board the vessel, with data recorded at a resolution of 1 s (Haas, 2020; Kanzow, 2020; Rex, 2020; Rex, 2021a, 2021b).

For this study, we excluded transit periods from the analyses, encompassing periods when *RV Polarstern* was in open water or breaking ice. Ice breaking and open ocean transit can lead to the measurements of fluorescent particles that would not represent the ice-covered ocean environment that we focus on. The ocean began to freeze up in early October 2019, while the onset of melt occurred toward the end of May 2020 (Salganik et al., 2023).

## 2.2. Sampling location and instrumental setup

The WIBS instrument was part of a comprehensive set of instruments housed in the *Swiss container*, located on the ship's foredeck (Beck et al., 2022a). Ambient aerosol and trace gases were sampled through 3 different sampling inlets, where two of which are relevant in this context. The first inlet, a whole air or total inlet, had an upper particle size cutoff of 40  $\mu\text{m}$  (World Meteorological Organization, 2016). The second inlet, an interstitial inlet, had an upper particle size cutoff of 1  $\mu\text{m}$ , allowing for the sampling aerosols that did not activate in ground-touching clouds or fog. A valve inside the container automatically switched between the total and interstitial inlets hourly. This allowed selected instruments, such as CCN counter, scanning mobility particle sizer, aerosol mass spectrometer (AMS), and aethalometer to alternate their sampling between the 2 inlets. The sample flows through the inlets were maintained at rates greater than 15 L/min for the total inlet and greater than 16.7 L/min for the interstitial inlet. The inlets were 1.5 m above the container, corresponding to around 15 m above sea level. The temperature and relative humidity in the inlet lines were maintained at around 20°C and below 40% RH. For more detailed information regarding the aerosol instrumentation inside the *Swiss container*, please refer

**Table 1. Fluorescent particle type classification as defined in Perring et al. (2015), with corresponding excitation-emission wavelength**

Particle Type	Excitation Wavelength [nm]	Emission Wavelength [nm]	Associated Aerosol (Savage et al., 2017)
A	280	310–400	Bacteria and fungi
B	280	420–650	Wood smoke and polycyclic aromatic hydrocarbons
C	370	420–650	Pollen, fungi, and humic-like substances
AB	280	310–400, 420–650	Bacteria and fungi
AC	280, 370	310–400, 420–650	unknown
BC	280, 370	420–650	Wood smoke and polycyclic aromatic hydrocarbons
ABC	280, 370	310–400, 420–650	Fungi and pollen

to Heutte et al. (2023). Angot et al. (2022d) provide detailed information on the trace gas measurements conducted in the *Swiss container*.

### 2.3. Measurement of FA

We used a WIBS to measure FA. While we briefly describe the WIBS here, a more detailed description of its predecessor model, which shares the same measurement principle, can be found in Gabey et al. (2010) and Savage et al. (2017).

The WIBS sampled from the total inlet, operating with a sample flow of 0.3 L/min and an internally generated particle-free sheath flow of 2.1 L/min. The inlet line from the total inlet to the WIBS was kept as straight and short as possible (2.5 m), resulting in estimated losses at the position of the WIBS from approximately 0% to approximately 4% for particles smaller than 3  $\mu\text{m}$ , from approximately 4% to approximately 10% for particles between 3 and 5  $\mu\text{m}$ , and from approximately 10% to approximately 35% for particles between 5 and 10  $\mu\text{m}$  (Heutte et al., 2023). No transmission corrections were applied. The WIBS functions as a single-particle instrument, using a 635-nm laser to measure the optical diameter of aerosols ranging from 0.5 to 30  $\mu\text{m}$  (here, we report only up to 20  $\mu\text{m}$ ). The correct sizing of the instrument was verified before deployment in the laboratory by measuring 1- and 3- $\mu\text{m}$  polystyrene latex spheres (PSL) for 1 h each. The measurements of 1- $\mu\text{m}$  PSL showed a mode in the size bin of 0.87–1.15  $\mu\text{m}$ , while the measurements of 3- $\mu\text{m}$  PSL exhibited a mode in the size bin of 2.63–3.16  $\mu\text{m}$ . The interaction of aerosols with the continuous 635-nm laser beam triggers 2 sequential UV xenon flash lamps at 280 and 370 nm to excite the aerosols. Two wideband detectors (FL1 and FL2) measure the emitted signal from the excited aerosols (EA) in the wavelength ranges of 310–400 and 420–650 nm, respectively. The excitation-emission wavebands of the WIBS are designed to detect specific biofluorophores, such as tryptophan (excitation wavelength 280 nm and emission waveband 300–350 nm), NADH (excitation wavelength 340 nm and emission waveband 420–530 nm), and riboflavin (excitation wavelength 350–500 nm and emission waveband 490–580 nm) (Pöhlker et al., 2012). Tryptophan is an amino acid found

in proteins and all biological cells, while NADH, a coenzyme, and riboflavin, also known as vitamin B2, are only contained in metabolizing organisms (Pöhlker et al., 2012). There are also other biofluorophores with excitation and emission wavelengths overlapping those mentioned above (Pöhlker et al., 2012).

Combining the 2 excitation wavelengths with the 2 emission wavebands allows the classification of 7 different fluorescent particle types using the notation introduced by Perring et al. (2015). Type A particles are excited at 280 nm and detected solely at FL1, type B particles are excited at 280 nm and detected solely at FL2, and type C particles are excited at 370 nm and detected solely at FL2. The remaining 4 types (AB, AC, BC, and ABC) result from the combinations of these 3 types, as described in **Table 1**. Note that each FA is assigned to only one of these 7 classes. It should be noted that FL1 becomes saturated when the 370-nm flash lamp is triggered, rendering it unable to contribute to the measurement.

Zero particle measurements using a high-efficiency particulate absorbing filter were conducted weekly for 1 h to verify the zero point of the WIBS. Additionally, “forced trigger” (FT) measurements were performed every 26 h for 5 min. During these FT measurements, both flash lamps were triggered without particles in the measurement chamber to determine the background fluorescence.

Following the approach of Gabey et al. (2010), we define FA as those whose fluorescence intensity exceeds the mean FT fluorescence signal by 3 standard deviations ( $\sigma$ ). Furthermore, following Savage et al. (2017), who found that using a threshold of the mean FT signal plus  $9\sigma$  reduces the contribution of nonbiological aerosols compared to FA, we employ this threshold to define hyperfluorescent aerosols (HFA). It is important to note that this method can also exclude biological aerosols that do not fluoresce strongly enough. The total number of particles triggering the UV flash lamps is called EA. The maximum detectable excited particle concentration of the WIBS is  $466 \text{ cm}^{-3}$ . HFA is a subset of FA, and FA is a subset of EA.

The WIBS data were processed using the WIBS IGOR toolkit V1.36 (Droplet Measurement Technologies, Longmont, CO, USA). The processed data include a size-resolved

number concentration calculated across 20 logarithmically equidistant optical diameter bins ranging from 0.5 to 20  $\mu\text{m}$ . We averaged the WIBS data over a 1-h time window for our analysis. Data are available on PANGAEA (Beck et al., 2023). The FT background fluorescence was stable throughout the year. To account for a decline of less than 10% between the first and the last FT measurements during MOSAiC, we determined the FT background data for each month individually.

#### 2.4. Removal of polluted and nonrepresentative data

The measurements in the *Swiss container* were regularly affected by local pollution from the ship's stack exhaust and activities, such as snowmobiles and small diesel generators (Beck et al., 2022a). The exhaust emissions contained fluorescent compounds like diesel soot and polycyclic aromatic hydrocarbons (PAHs), which emit signals within the WIBS detection range (Savage et al., 2017). In Section S1, we quantify the impact of local pollution on FA. Figures S1 and S2 demonstrate that ship exhaust predominantly affects fluorescent types A, AB, and ABC. To ensure accurate measurement of natural FA (biological and nonbiological), it is crucial to exclude identified polluted periods. We applied a pollution mask developed by Beck et al. (2022a) based on the particle number concentration data from a condensation particle counter (TSI Inc., Shoreview, MN, USA, Model 3025) installed in the *Swiss container* (Beck et al., 2022b). By removing polluted periods, we reduced the initial data set from 8,267 to 2,698 hourly data points, a 68% reduction. To focus on the Arctic Sea ice environment, we excluded periods when the ship was in transit, either in open water (191 h) or ice-breaking (125 h). Zero particle measurements and periods not representative of ambient conditions (e.g., when the sampling inlet was opened briefly) were also excluded from the data set. This resulted in a final data set of 2,298 hourly data points. Only days with a minimum of 8 h of usable data were included for calculating daily averages. The hours can be consecutive or randomly distributed over 1 day.

#### 2.5. Ancillary measurements

##### 2.5.1. Atmospheric aerosol and trace gas measurements

Equivalent black carbon (eBC) was measured using the Aethalometer AE33 (Magee Scientific, Berkeley, USA) that acquired data at a resolution of 1 s. The AE33 collects aerosols on a filter tape and estimates the eBC mass concentration by measuring the light absorption coefficient at 7 wavelengths. Biweekly zero particle measurements were conducted during the expedition. The data underwent pollution and quality control and were subsequently averaged to a 10-min resolution (Heutte et al., 2022), following the procedure outlined in Heutte et al. (2023). In this study, we used the hourly mean values of the signal at 880 nm as an indicator of Arctic haze (Boyer et al., 2023).

Submicron sodium chloride (NaCl) mass concentrations were estimated with a time resolution of 3 min and are derived from the measurements of a high-resolution time-

of-flight AMS (Aerodyne Research Inc., DeCarlo et al., 2006). The AMS measures the mass concentration and chemical composition of nonrefractory aerosols (those that evaporate at  $\leq 600^\circ\text{C}$ ) smaller than 1- $\mu\text{m}$  vacuum aerodynamic diameter. NaCl concentrations were estimated based on the  $^{23}\text{Na}^{35}\text{Cl}^+$  fragment signal at the mass-to-charge-ratio ( $m/z$ ) 58, and the obtained mass concentrations were multiplied by a factor of 51, following the method proposed by Ovadnevaite et al. (2012). The NaCl concentration provided is an estimate only because the AMS cannot detect refractory aerosols without artifacts. NaCl concentration estimates were averaged to 1-h resolution. The AMS calibration was conducted before and during the expedition, and biweekly zero particle measurements were performed throughout the expedition (Heutte et al., 2023).

Particles were collected for offline measurements of INP number concentrations over 4 different size ranges (3–12  $\mu\text{m}$ , 1.2–3  $\mu\text{m}$ , 340 nm–1.2  $\mu\text{m}$ , and 150–340 nm) using a Davis Rotating-drum Unit for Monitoring (DRUM, model DA-400, DRUMAir) impactor. INPs were measured using a cold plate freezing assay from Colorado State University and concentrations were calculated based on Vali (1971). Further information is provided by Creamean et al. (2022). The data have been published in Creamean et al. (2022) and Creamean (2021). The DRUM instrument was situated in the U.S. Department of Energy Atmospheric Radiation Measurement program's Aerosol Observing System (AOS) container, opposite the *Swiss container* on the front deck of *RV Polarstern*. Please refer to Uin et al. (2019) for a detailed overview of the AOS container. To ensure representative measurements, a subset of INP samples collected over 24 h were analyzed, providing one measurement every third day. INP concentrations were recorded down to a temperature of  $-29^\circ\text{C}$  with  $0.5^\circ\text{C}$  temperature intervals, employing an immersion-freezing method as outlined in Creamean et al. (2022). For this study, we excluded the smallest size bin of INPs and used the total INP concentrations spanning the size range of 340 nm to 12  $\mu\text{m}$ , which aligns best with the size range covered by the WIBS.

##### 2.5.2. Meteorological data

Meteorological data are at 1-min time resolution and were collected aboard *RV Polarstern* (Shupe et al., 2022). Wind direction and speed measurements were obtained at a height of 39 meters above sea level (m.a.s.l.) using a 2D sonic anemometer (Thies Clima) installed on the vessel's main mast. Temperature readings were recorded at 29 m.a.s.l., using a Vaisala HMP155 thermometer, while pressure data were obtained from a Setra B270 barometer at 29 m.a.s.l. (Schmithuesen, 2021a, 2021b, 2021c, 2021d, 2021e).

##### 2.5.3. Other data

Sea water samples for chlorophyll a (Chl-a) analysis were extracted from a seawater intake at a depth of 11 m and filtered onto 0.7- $\mu\text{m}$  glass fiber filters (grade GF/F). The filters were stored frozen at  $-80^\circ\text{C}$  until analysis at the Alfred Wegener Institute after the expedition. Multiple

samples per week were homogenized and extracted in 90% acetone overnight before being analyzed with a fluorometer (TD-700, Turner Designs, USA) to detect Chl-a fluorescence-derived concentrations (Knap et al., 1996).

Daily thermal infrared satellite images, taken by the Moderate Resolution Imaging Spectroradiometer, were derived by the University of Trier and used to identify leads in the ice. The lead fraction product was calculated at a spatial resolution of 12.5 km<sup>2</sup>, as described by Reiser et al. (2020). The data represent a 1 \* 1-degree grid box around *RV Polarstern* and cover the period between November 2019 and April 2020 (Willmes et al., 2023).

Daily averaged melt pond fractions in a 1 \* 1 degree grid box around *RV Polarstern* were identified using optical imagery from the Sentinel-3 satellite at a spatial resolution of 12.5 km<sup>2</sup> (Istomina, 2020). The melt pond fraction data are available between May and August 2020.

The size distribution of airborne snow particles ranging from 36 to 490 μm was measured by an open-path snow particle counter (SPC-95; Niigata Electric Co., Ltd) and used to compute snowdrift density (snow mass per volume of air). Two SPCs were set up at nominal heights of 0.1 and 10 m above the snow surface on a mast on the ice floe to which *RV Polarstern* was moored. Data are available from Frey et al. (2023). Blowing snow events were classified according to Li and Pomeroy (1997).

## 2.6. FLEXPART simulations

To identify the source regions of air masses, we utilized aerosol tracer simulations performed at the University of Vienna using the FLEXPART v10.4 Lagrangian particle dispersion model (Pisso et al., 2019). These simulations specifically focused on the aerosol tracer SO<sub>4</sub><sup>2-</sup> and considered both wet and dry deposition of aerosols. The simulations used the hourly ERA5 meteorological reanalysis data with a spatial resolution of 0.5° × 0.5°. In the simulations, a cluster of 100,000 particles was released every 3 h at the position of *RV Polarstern* and traced backward for 7 days. The resulting residence time of air masses (footprints) over the geographic grid of the lowest 100 m of the atmosphere was then used to investigate the source regions of air masses on specific days. The model outputs for the entire expedition can be accessed at <https://img.univie.ac.at/webdata/mosaic>. Additionally, the relative contribution of particular surfaces, such as the ocean, ice, Greenland, North America, North Asia, and Europe, is calculated. In the case of ice, the relative contribution is directly proportional to the fraction of sea ice cover over the geographical grid encountered by the air masses. The ocean represents the ice-free ocean contribution in this article. This analysis allowed us to visualize the influences from different regions throughout the year.

## 3. Results and discussion

### 3.1. Annual cycle of FA

**Figure 2** shows the monthly mean concentrations of EA, FA, and HFA ( $N_{EA}$ ,  $N_{FA}$ , and  $N_{HFA}$ ) throughout the MOSAiC campaign in panels (a)–(c). It also includes the fractions of FA and HFA in relation to EA ( $f_{FA}$  and  $f_{HFA}$ ) and the ratio of  $N_{HFA}$  to  $N_{FA}$  ( $f_{HFA/FA}$ ).  $N_{EA}$ ,  $N_{FA}$ , and  $N_{HFA}$  exhibit the typical

annual cycle of Arctic coarse and accumulation aerosols with higher concentrations during the Arctic haze season (November to April) and lower values in October 2019 and between June and September 2020 (e.g., Song et al., 2021; Boyer et al., 2023). The highest monthly median values (lower and upper quartiles) for  $N_{FA}$  and  $N_{HFA}$  were 173 (118, 229) L<sup>-1</sup> and 13 (8, 18) L<sup>-1</sup>, respectively, occurring in January. The lowest monthly median (lower and upper quartiles) values for  $N_{FA}$  and  $N_{HFA}$  were 1.3 (0.6, 2.9) and 0.3 (0.1, 0.8) L<sup>-1</sup>, occurring in August. This indicates that FA and HFA observed between November and April are likely influenced by the Arctic haze, which includes nonbiological FA like black carbon (Savage et al., 2017). The relationship between FA and Arctic haze is discussed in Section 3.2. Taketani et al. (2022) observed  $N_{HFA}$ , using a WIBS-4, in the Northwest Pacific, the Bering Strait, and the Arctic Ocean from a research vessel between August and October 2016. They found a mean  $N_{HFA}$  of 680 ± 580 L<sup>-1</sup> at latitudes > 70°N, which is higher than our observations.

The  $f_{FA}$  and  $f_{HFA}$  are consistently higher between June and October than between November and May (**Figure 2d** and **e**). The maximum values for  $f_{FA}$  and  $f_{HFA}$  were 0.18 and 0.1, respectively, occurring in June 2020. The minimum values were 0.03 and 0.0016, respectively, occurring in April and May. This suggests that FA and HFA do not represent a constant subset of the EA throughout the year, but various sources and processes lead to substantial variability. In addition, from June to October, both  $f_{HFA}$  and  $f_{FA}$  demonstrated larger variability with high-fraction outliers, as indicated by larger interquartile range values and noticeable differences between mean and median values compared to the period from November to May. Conversely, the fractions are more stable during the November to April period, with fewer high-fraction events, resulting in more minor variability and higher similarity between mean and median values. Further details regarding the variability of FA measurements during different campaign periods are discussed in Section 3.1.2. The highest  $f_{HFA}$  found by Taketani et al. (2022) was observed in September in the Bering Strait in the range of 0.15–0.25. This is comparable to our highest observations in summer.

**Figure 2f** shows  $f_{HFA/FA}$ , which remains relatively stable at around 0.08 between November and April and peaks at 0.7 in June. The strong differences in  $f_{HFA/FA}$  values between the November–April and June–August periods suggest varying sources of FA and HFA throughout the year in the Arctic, with HFA being more strongly influenced by biological sources, which is consistent with previous studies (Savage et al., 2017; Moallemi et al., 2021). Since HFA are less influenced by nonbiological sources than FA and are better suited to describe biological aerosols, we focus mainly on HFA in this study.

### 3.1.1. Fluorescence type contributions

The contribution of different types of FA throughout the year can provide insights into their potential sources. **Figure 3a** shows the annual cycle of HFA type contributions to the total HFA concentration. It reveals distinct and somewhat opposing patterns of fluorescence types: Types B and BC are most prominent between November and

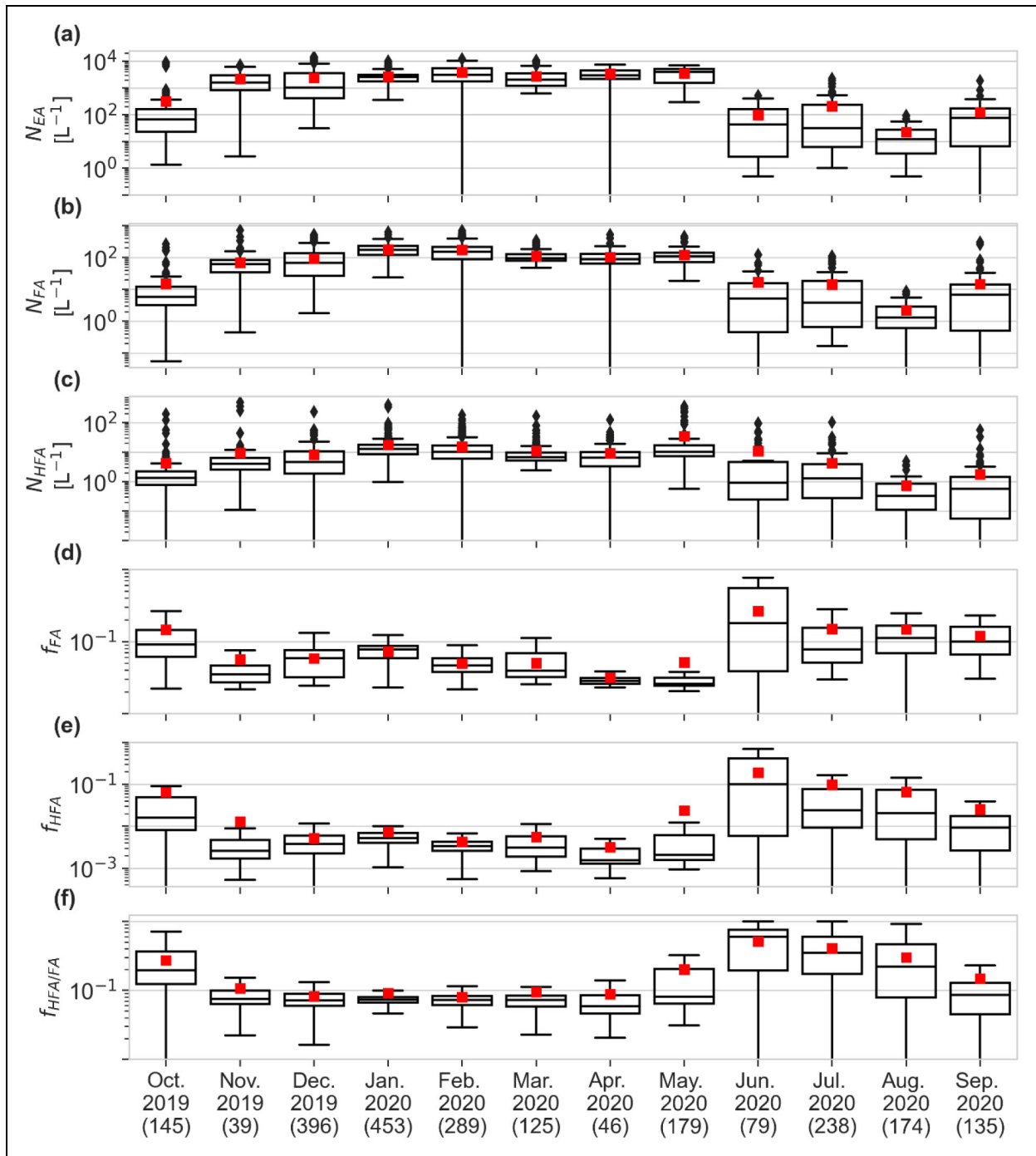


**Figure 2. Annual cycle of excited, fluorescent, and hyperfluorescent aerosol concentrations and fractions.** Monthly boxplots of number concentrations of excited ( $N_{EA}$ , a), fluorescent ( $N_{FA}$ , b), and hyperfluorescent ( $N_{HFA}$ , c) aerosols as well as of their fractions of  $N_{EA}$  ( $f_{FA}$  and  $f_{HFA}$ , d and e) and the ratio  $f_{HFA/FA}$  (f). The red dots show the monthly mean values. The boxes cover the interquartile range and show the median values as vertical lines, and the whiskers show the 2.5th and 97.5th percentile. Each month's hourly average data points are shown in brackets.

April and in September, while types A and AB appear more pronounced from May to August. Type ABC is most pronounced in July and August and also contributes in September and December. Type AC is absent throughout the year, and type C contributes only little to the HFA in general and not at all in June. Comparing the fluorescence type contributions (Figure 3) and number concentration (Figures 2 and S3) from October, they appear more similar to those from June to August than those from

November to April and September. Note that the October measurements were obtained in 2019, while the September samples were measured in 2020. Differences in sampling location (85°N, 130°E in October 2019 and 88°N, 120°E in September 2020) and environmental factors, such as the predominant air mass origin and algal bloom presence, could contribute to the distinct characteristics of the data in October 2019. Further discussion on this observation is provided in Section 3.5.



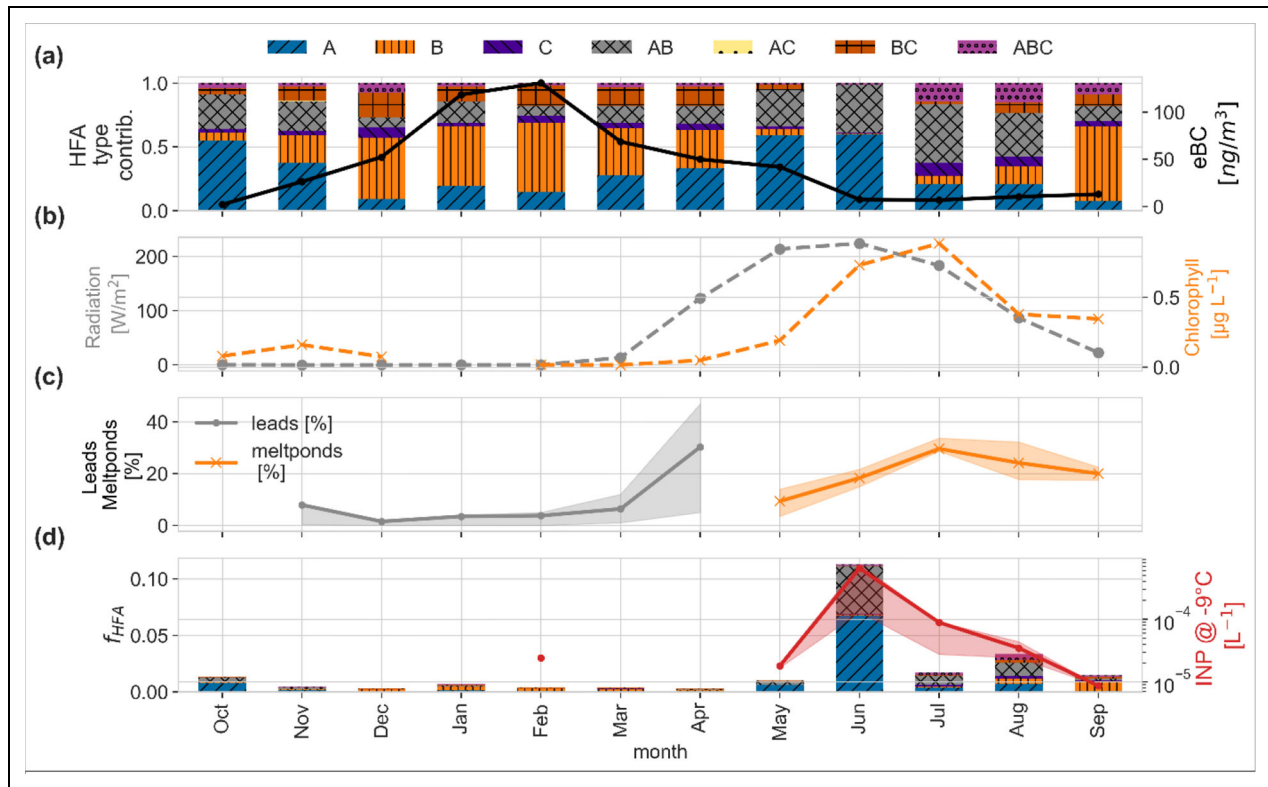


**Figure 3. Annual cycle of fluorescence type contributions to hyperfluorescent aerosols (HFA), compared to selected ancillary data.** Monthly mean values (October 2019–September 2020) of different fluorescence type contributions to HFA (a). Each type corresponds to a specific excitation-emission wavelength combination, as in **Table 1**. The black line in (a) shows the monthly mean equivalent black carbon (eBC) concentrations. Panel (b) shows the monthly mean global radiation (in gray, left  $y$ -axis) and Chl-a concentrations from 11 m below the sea surface (in orange, right  $y$ -axis). The melt onset was around May 25, 2020, and the freeze-up was around September 8, 2020 (Salganik et al., 2023). Panel (c) shows the lead and the melt pond fractions. Panel (d) shows  $f_{\text{HFA}}$  of all types (left axis) and the INP concentration at  $-9^{\circ}\text{C}$  (right axis, in red). Please see Figure S3 for the absolute concentrations of fluorescent FA and HFA types and Figure S4 for higher time resolution data of the ancillary data (panels c–e here).

### 3.1.2. Three characteristic periods

Based on the distinct patterns of  $N_{\text{HFA}}$ ,  $f_{\text{HFA}}$ , and HFA fluorescence types, we divided the annual cycle into 3 periods, as indicated on the  $x$ -axis in **Figure 4**.

Period 1 (November 2019–April 2020 and September 2020) covers the Arctic Haze season and is characterized by relatively high  $N_{\text{HFA}}$  (median of  $7 \text{ L}^{-1}$ ), low  $f_{\text{HFA}}$  (0.003) (**Figure 2**), and the dominance of type B (46%), with the remaining type contributions as follows: type A: 19%, type C: 5%, type AB: 12%, type BC: 15%, and type ABC: 3% (Figure S5). Despite the low  $f_{\text{HFA}}$  values in period 1, occasional events with  $f_{\text{HFA}}$  reaching values as high as 0.05 occurred, and these events (bursts) had a distinct composition of fluorescence types compared to the average of period 1. In total, we identified 5 events (numbered in **Figure 4**), where the criteria for an event are (i)  $f_{\text{HFA}}$  is larger than the 90th percentile of  $f_{\text{HFA}}$  in period 1 and (ii) the sum of fractions of types A, AB, and ABC must exceed 0.5 (see Section S3 for more details). The average high- $f_{\text{HFA}}$  burst duration was around 12 h. We discuss the events in Section 3.3. Overall, period 1 can be characterized by a steady level of HFA, dominated by type B, occasionally interrupted by events with higher  $f_{\text{HFA}}$  and strong type A and AB contributions.

Period 2 (May 2020–August 2020) is characterized by relatively low median  $N_{\text{HFA}}$  ( $1.9 \text{ L}^{-1}$ ), high median  $f_{\text{HFA}}$  (0.012), and the dominance of types A and AB. It corresponds to the Arctic summer season, where we observed the lowest concentrations of EA (**Figure 2**). However, despite the lower aerosol number concentration, the relative difference between  $N_{\text{EA}}$  and  $N_{\text{HFA}}$  was smaller, compared to period 1, causing the higher proportions of  $f_{\text{HFA}}$ . As depicted in **Figure 4**, the daily variations of HFA fluorescence types were more diverse and exhibited higher variability compared to period 1. The occurrence of days with high  $f_{\text{HFA}}$  in period 2 appeared to be of longer duration than the period 1 events, contrasting the relatively stable fluorescent background nature of period 1, which was only occasionally interrupted by events. The predominant HFA types in period 2 were A (54%) and AB (32%) (Figure S5). The variability and the overall higher  $f_{\text{HFA}}$  suggest that the sources of HFA in period 2 differ from the Arctic haze background in period 1 and may be more similar to the high- $f_{\text{HFA}}$  events observed in period 1.

Period 3 (October 2019) stands out due to the distinct fluorescence properties of aerosols in combination with the absence of solar radiation and ongoing freeze-up. During this period, there was low  $N_{\text{HFA}}$  ( $1.4 \text{ L}^{-1}$ ), but a high

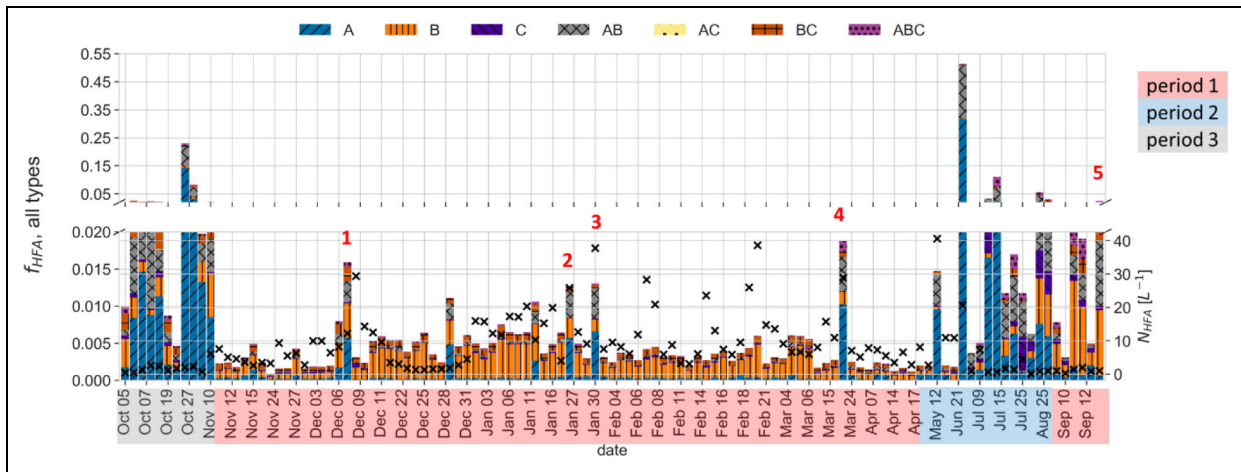


**Figure 4. Daily fraction of hyperfluorescent aerosols (HFA; 114 days), separated by fluorescence types.** Daily mean fraction of HFA ( $f_{\text{HFA}}$ ) to excited aerosols. Each bar is split based on the contribution of the different fluorescence types. The  $y$ -axis is split to enlarge the lower concentrations. Note that the  $x$ -axis labels do not represent every single bar in the figure and that the time series contains gaps due to missing or polluted data. Missing days experienced ship pollution beyond the threshold of 8 h with valid data points per day, as defined in Section 2.4, and are hence not considered. The dates are in chronological order and start in October 2019. The numbers indicate identified events of relatively high  $f_{\text{HFA}}$ , as discussed in Section 3.3. The height of the bars corresponds to their fraction. The right  $y$ -axis in the lower panel shows the HFA concentration ( $N_{\text{HFA}}$ ), indicated by black crosses. The 3 periods are highlighted in the  $x$ -axis: period 1 in red, period 2 in blue, and period 3 in gray. Periods 2 and 3 show similarities in terms of fluorescent type contributions but are discussed separately as period 3 was during the polar night in 2019 and period 2 was during the polar day in 2020. A similar figure, including all gaps, is provided in the SI, Figure S6.

$f_{\text{HFA}}$  of 0.012, dominated by types A (51%) and AB (28%) of the HFA (Figure S5). The type composition and  $f_{\text{HFA}}$  were more similar to period 2 and distinct from September 2020, which falls under period 1. In contrast to period 2, this period occurred in a different geographical region (Figure 1) and in a time without sunlight. After November 10,  $f_{\text{HFA}}$  sharply decreased from 2% to 0.2%, initiating period 1 (Figure 4).

### 3.2. Anthropogenic influence on FA in winter and spring

In the central Arctic, FA abundance can be driven by a variety of sources, for example, anthropogenic versus biogenic and long distance versus local, and different production mechanisms. This and the following sections investigate different sources and emission processes of FA.

Figures 2c and 3a indicate a covariance between eBC mass concentration and  $N_{\text{HFA}}$  and the type composition of HFA, as well as specific fluorescence types, particularly type B. To further explore the connection between eBC and HFA, we conducted a correlation analysis between hourly eBC and HFA measurements (Figure 5). We observed a strong correlation between eBC and  $N_{\text{HFA}}$  during period 1 (Spearman rank  $r = 0.85$ ) and moderate correlations during periods 2 ( $r = 0.49$ ) and 3 ( $r = 0.36$ ). Among all fluorescence types,  $N_{\text{HFA, B}}$  and  $N_{\text{HFA, BC}}$  exhibited the highest correlations with eBC in all periods, with  $r_{\text{B}} = 0.88$  and  $r_{\text{BC}} = 0.83$  in period 1,  $r_{\text{B}} = 0.7$  and  $r_{\text{BC}} = 0.67$  in period 2, and  $r_{\text{B}} = 0.44$  and  $r_{\text{BC}} = 0.36$  in period 3. An ambient aerosol study conducted in an urban area

by Yue et al. (2022) showed that types B and BC are strongly associated with nonbiological fluorescent particles, such as combustion emissions and secondary organic aerosols. The presence of eBC is considered a characteristic feature of Arctic haze (Quinn et al., 2007; Bond et al., 2013; Schmale et al., 2022; Boyer et al., 2023). Typically, Arctic haze peaks in late winter (Barrie, 1986; Schmale et al., 2022). However, during MOSAiC, we observed an unusually early peak of eBC in January. This early peak has been attributed to a strong positive anomaly of the Arctic Oscillation, which increased the transport of air masses from lower latitudes into the central Arctic (Rinke et al., 2021; Boyer et al., 2023). Our observations of type B contributions to FA and HFA reflect this with high values in January (Figure S3).

We conclude that types B and BC are likely influenced by anthropogenic sources, consistent with the findings of Hernandez et al. (2016) and Yue et al. (2022), who suggest that atmospheric measurements, in which type B is a dominant fluorescence type, have nonbiological interferences. Type B has also been associated with biomass burning and PAHs, typically emitted from anthropogenic sources, by Savage et al. (2017). Both PAHs and emissions from domestic wood combustion are known and significant contributors to Arctic haze (Halsall et al., 1997; Stohl et al., 2013). Our bubble-bursting experiments with seawater indicate that sea spray and dissolved organic matter might also be related to type B (SI Section 4, Figure S12), and their contribution to period 1 cannot be ruled out.

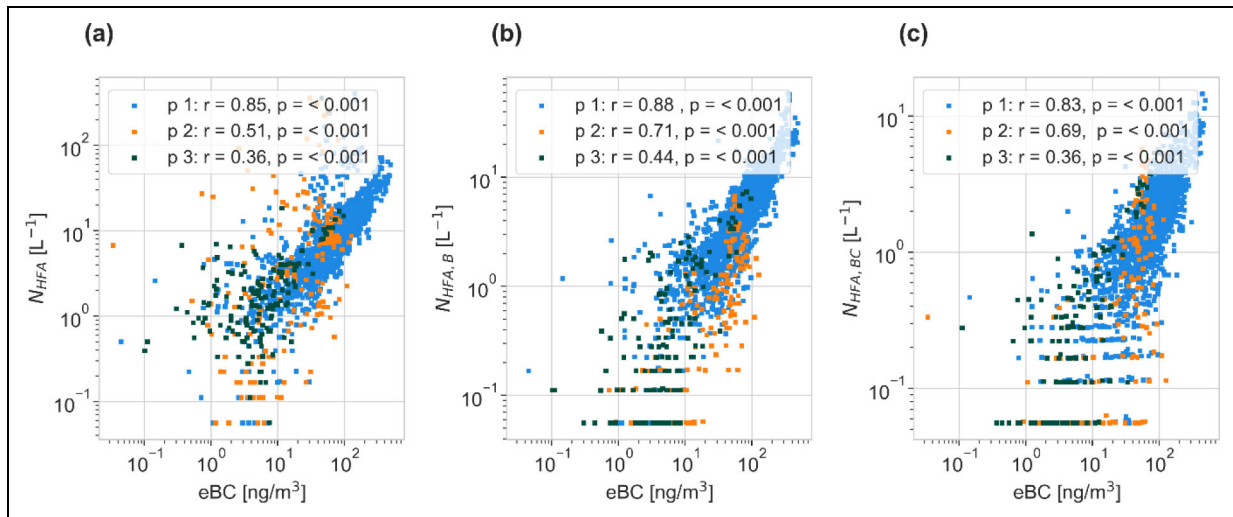


**Figure 5. Correlation between black carbon and selected hyperfluorescent aerosol (HFA) concentration in 3 periods.** The total HFA concentration ( $N_{HFA}$ , a) and that of type B ( $N_{HFA,B}$ , b), and type BC ( $N_{HFA,BC}$ , c) against equivalent black carbon (eBC) concentrations for all 3 periods (period 1—p 1 in blue, p 2 in orange, and p 3 in green). Spearman correlation ranks are provided for each period and each HFA type.

### 3.3. Potential contribution of biological sources to FA events in winter and spring

The 5 high- $f_{HFA}$  events in period 1 (Sections 3.1.2 and S3) are characterized by high type A contribution (Figure 4), while period 1 is generally dominated by type B FA. The origin of air masses during the events is similar to other days in period 1 (see Figure S7). Figure S7 indicates that land sources minimally influenced the events, while the influence of ice and open ocean on the air masses was most prominent. This suggests that air from within the central Arctic pack ice and ocean can contain relatively high fractions of—potentially biological—fluorescent type A particles, even during period 1. Size distributions of fluorescent type A and other types might provide an additional indication of the origin, since PBAP, and in particular bacteria, can be found in the size range of  $<1 \mu\text{m}$  to roughly  $3 \mu\text{m}$  with the WIBS (Hernandez et al., 2016; Savage et al., 2017). The mean size distributions of EA and all HFA types during each event are shown in Figure S8, and a combined mean size distribution of all events is shown in Figure S9. The size distributions during the events in period 1 show considerable variability, whereas the size distributions during events 2–4 show a mode in type A HFA around  $2\text{--}3 \mu\text{m}$ . Event 5 shows a strong mode of HFA of type ABC between  $0.8$  and  $2 \mu\text{m}$ . This may support the potential biological origin of FA during the events. Only event 1 shows a strong mode of types B and BC at sizes  $>1 \mu\text{m}$ , which might indicate a potential anthropogenic influence.

These findings are notable, as large parts of period 1 are characterized by the absence of sunlight, as depicted in Figure 3b, and generally expected low biological activity (Wassmann and Reigstad, 2011; Berge et al., 2015). Nevertheless, Berge et al. (2015) reported unexpectedly high biological activity without photosynthetic production in a fjord of Svalbard. Algal and bacterial communities, as well as remnants of their past activities, are known

to exist in the ice in winter (Junge et al., 2004; Olsen et al., 2017; Thiele et al., 2022; Torstensson et al., 2023). These microorganisms could potentially be released into the atmosphere from open leads or ridging events, providing a local PBAP source. Fernández-Méndez et al. (2018) discovered high algal accumulation in first-year-ice ridges in the Arctic Ocean northwest of Svalbard. This led to significantly higher biomass concentrations than typically found in undeformed (level) ice. While there is, hence, evidence that microorganisms are present in the ocean and the sea ice in the central Arctic during period 1, to the best of our knowledge, there are currently no studies available that investigate the process of microorganism aerosolization from the ice and in particular ridges into the atmosphere, which would provide further evidence supporting this specific mechanism. Moreover, the marginal ice zone with open water could be another source. Our data also cannot exclude longer range transport from midlatitudes responsible for episodic “bursts” of type A fractional contributions.

Another potential source of the HFA during these events may arise from precipitating and sublimating ice crystals, liberating PBAPs, which previously acted as INPs. These PBAPs could potentially originate from regions at lower latitudes and have been transported into the central Arctic. However, this hypothesis requires further investigation.

### 3.4. The influence of wind speed on FA

The Arctic experiences high wind speeds, particularly in winter, and during the MOSAiC year several abnormally strong storms were observed (Rinke et al., 2021; Shupe et al., 2022). Wind-induced aerosol generation could, therefore, be a relevant contribution to FA abundance. In Figure 6, we show that  $N_{HFA}$  increases with increasing wind speed, while  $f_{HFA}$  decreases. Two mechanisms related to wind speed could potentially influence the HFA:

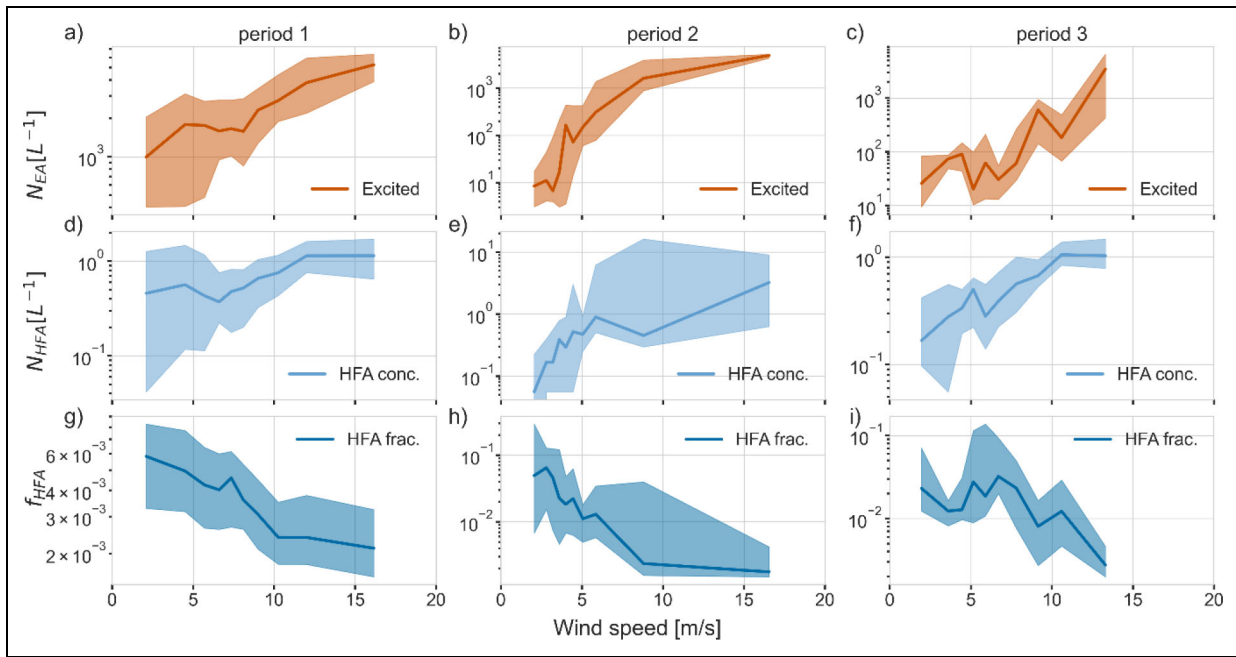


**Figure 6. Investigation of the influence of wind speed on excited aerosols (EA) and hyperfluorescent aerosols (HFA).** The number concentration of EA ( $N_{EA}$ , a–c) and of HFA ( $N_{HFA}$ , d–f) concentrations and the fraction of HFA ( $f_{HFA}$ , g–i) against wind speed for all 3 defined periods. The interquartile range is presented in the shaded areas.

(i) blowing snow and (ii) SSA generation from leads, polynyas, and open ocean. In this section, we discuss these 2 mechanisms and laboratory-based bubble-bursting experiments explicitly conducted to aid the interpretation of the fluorescence data (Section S4).

Snow accumulates on sea ice, and under high wind speeds, snow grains can be lifted into the atmosphere (blowing snow), subsequently sublimating, leaving behind snow impurities in the form of aerosols. Those are suggested to be primarily sea salt particles (Frey et al., 2020). Focusing on period 1, which coincides with favorable conditions for blowing snow and exhibits sporadic events of high- $f_{HFA}$ , we compared  $f_{HFA}$  and relative contributions of all types during period 1 under blowing snow and non-blowing snow conditions. We observe that blowing snow does not enhance  $f_{HFA}$  (Figure S10), and the type compositions are comparable between blowing snow and non-blowing snow periods (Figure S10b). Additionally, only one of the high  $f_{HFA}$  events in period 1 occurred at the same time as blowing snow was observed, suggesting that the events with high  $f_{HFA}$  in period 1 were not induced by blowing snow.

About the second mechanism, high wind speeds can release SSA from leads and polynyas (Scott and Levin, 1972; Nilsson et al., 2001; Leck et al., 2002; May et al., 2016; Kirpes et al., 2019), as well as the open ocean, contributing to fluorescent particle concentrations (Santander et al., 2021). SSA includes organic-dominant particles, sea salt with varying amounts of organic material, and microorganisms (Prather et al., 2013). Emission of SSA is amplified at wind speeds above 5 m/s (de Leeuw et al., 2011; Quinn et al., 2015) when waves start to break, with SSA emissions further increasing with wind speed for both open water and leads (Nilsson et al., 2001). Therefore,

given suitable environmental conditions (i.e., sufficient marine biological biomass), higher wind speeds could enhance marine PBAP generation. We observed an increase in the number of  $N_{EA}$  and  $N_{HFA}$  with higher wind speeds in all periods (Figure 6). This was also observed in comparable studies over open ocean environments (Kawana et al., 2021; Moallemi et al., 2021; Kawana et al., 2024), suggesting a possible association between HFA and SSA generation.

To investigate the potential contribution of SSA to HFA during the MOSAiC campaign, we used the estimated particulate NaCl concentration measured by an AMS as a tracer for SSA and examined its relationship to  $N_{HFA}$  (Figure S11). The type B HFA and the estimated NaCl concentrations were correlated weakly in period 1 ( $r = 0.14$ ), more strongly in period 2 ( $r = 0.74$ ), and moderately in period 3 ( $r = 0.48$ ). The positive correlation with type B is consistent with our bubble bursting experiment (see description in Section S4): In the laboratory experiment, we investigated the fluorescence properties of nascent SSA using Baltic Sea water, which demonstrated that SSA was predominantly detected as type B (Figure S12). The fact that type B dominates the FA in filtered seawater (Figure S12b) indicates that type B is also associated with fluorescent dissolved organic matter. The relatively weak correlation of type B with NaCl in period 1 could be due to the association of fluorescent type B with Arctic haze, which was dominant during period 1. This highlights the limitation of the WIBS in distinguishing different aerosol sources if they have similar fluorescent properties. It is also important to note that SSA from Baltic Sea water likely has different properties and composition than SSA emitted from the high Arctic Ocean. The Baltic Sea has a lower salinity (our sample had a salinity of 6 g/L)

than the Arctic Ocean, which has a salinity of approximately 31–35 g/L (Hoppmann et al., 2022; Rabe et al., 2022; Schulz et al., 2023), and the salinity level is known to influence the fluorescent properties and emission of SSA (Mostofa et al., 2013; Zinke et al., 2022). There are further differences regarding water temperature and microbiology (microorganism types and activity), where the latter is not well quantified. These differences have an impact on the bubble-bursting process itself as well as on the composition of the SSA and the resulting fluorescent signal. There is, hence, a need for further bubble tank experiments with high-Arctic seawater.

Figure S11d shows that HFA type C correlated moderately with NaCl in all 3 periods ( $r = 0.61$ ,  $r = 0.69$ , and  $r = 0.47$ ). Type C FA have been associated with HULIS, but typically fluoresce only weakly (Savage et al., 2017; Santander et al., 2021). Thus, and because type C HFA only contributed little to the SSA in our laboratory experiment, it is unclear what causes the correlation between type C HFA and NaCl.

The above discussions referred to the observation that  $N_{HFA}$  increased with wind speed. However,  $f_{HFA}$  decreased with increasing wind speed (Figure 6g–i), indicating that while stronger winds are a source of HFA, they are a stronger source of EA. In other words, higher enrichment of

HFA is found under lower wind speed conditions. Section 3.7 discusses the possible release mechanisms of HFA under low-wind conditions.

### 3.5. Biological influence on FA in summer and fall

Periods 2 and 3 exhibit dominant contributions from fluorescence types A and AB, previously associated with bacteria, fungal spores, and algae (Perring et al., 2015; Savage et al., 2017). Building on this prior knowledge and in the absence of airborne measurements of bacteria, fungal spores, and algae, we investigate 2 aspects more thoroughly to establish the link between observations and potential biological sources: (i) the FA size distribution and (ii) the co-occurrence of INP that are active at elevated temperatures. Biological particles have characteristic sizes ( $>0.5 \mu\text{m}$ ) (Pöschl et al., 2010; Huffman et al., 2012; Fröhlich-Nowoisky et al., 2016), and warm INP are typically associated with PBAP (Després et al., 2012; Hartmann et al., 2020; Huang et al., 2021).

Figure 7 shows the period-averaged particle size distributions of EA, FA, and HFA (panels a–c), of  $HFA_A$ ,  $HFA_{AB}$ , and  $HFA_{ABC}$  (panels d–f), and the fractions of  $HFA_A$ ,  $HFA_{AB}$ , and  $HFA_{ABC}$  (panels g–i) in all 3 periods. During all 3 periods, the number size distributions of EA, FA, and HFA show a near-monotonic decrease with size (Figure 7a–c). However,

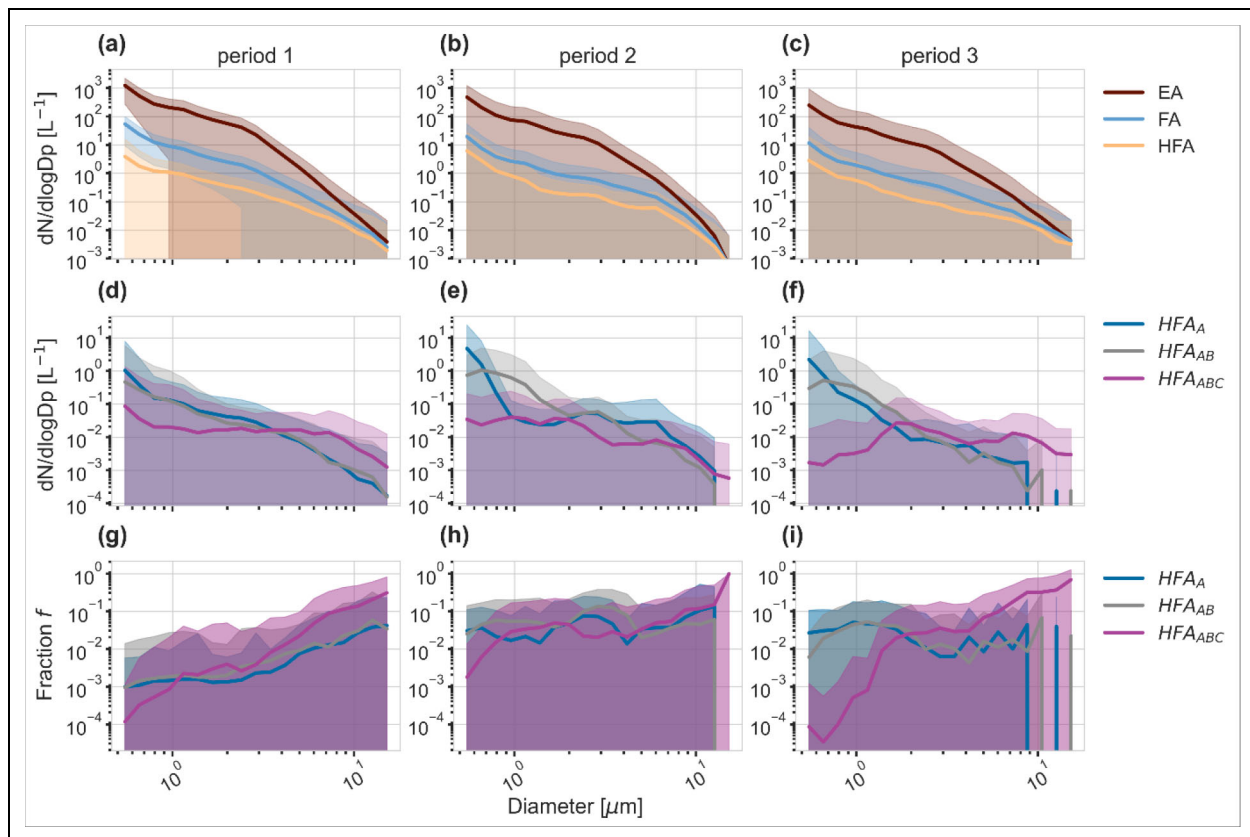


**Figure 7.** Size distributions of excited aerosols (EA), fluorescent aerosols (FA), and hyperfluorescent aerosols (HFA) concentrations and of the fractions of HFA. Size distributions of EA (brown), FA (blue), and HFA (orange) particle concentrations (a–c), of the concentrations of hyperfluorescent types A (blue), AB (gray), and ABC (purple) (d–f), and of hyperfluorescent fractions of type A (blue), type AB (gray), and type ABC (purple) (g–i) in all 3 periods. The lines and the shaded areas show the mean values and the standard deviation, respectively. The concentrations were normalized to the bin with the highest concentrations.

looking at the size distributions of  $HFA_A$ ,  $HFA_{AB}$ , and  $HFA_{ABC}$  (**Figure 7d–f**), we observe monotonic decreases of  $HFA_A$  and  $HFA_{AB}$  in period 1, while  $HFA_{ABC}$  plateau between 1 and 8  $\mu\text{m}$ . Periods 2 and 3 differ from period 1 in that the size distributions of  $HFA_{AB}$  show a distinct mode below 1  $\mu\text{m}$ . Furthermore, period 2 shows another distinct mode of  $HFA_{AB}$  and  $HFA_A$  between 2 and 3  $\mu\text{m}$ . While  $HFA_A$  do not show a mode in period 3, the small mode around 1  $\mu\text{m}$  of  $HFA_{AB}$  is also observed. The  $f_{HFA}$  of types A, AB, and ABC in **Figure 7g–i** also show the mode of  $HFA_A$  and  $HFA_{AB}$  between 2 and 3  $\mu\text{m}$  in period 2 and a mode around 1  $\mu\text{m}$  in period 3.

Previous studies have identified a size mode around 2–3  $\mu\text{m}$ , attributing it to biological particles (Pöschl et al., 2010; Després et al., 2012; Huffman et al., 2012; Freitas et al., 2022). Santander et al. (2021) demonstrated the presence of such a mode in aerosolized marine bacterial isolates. In Figure S13, we show example fluorescence microscopy maps from 3 dates in November 2019 and June 2020 to support the occurrence of  $>1.15\text{-}\mu\text{m}$  fluorescent particles in the size range detected by the WIBS with an independent method in both periods 1 and 2; note that these images do not show the presence of soot. As discussed in Section S5, this method has previously been used to identify biological material in ambient aerosols (Pöhlker et al., 2012) and in bubble-bursting aerosol from water impacted by an algal bloom (May et al., 2018). In our bubble tank experiment, we also identified a mode consisting of type A particles within the 0.8–3.5  $\mu\text{m}$  and of type AB particles within the 1–3  $\mu\text{m}$  size range when examining filtered seawater supplemented with bacteria (Figure S14). These findings suggest an association between HFA and PBAP in periods 2 and 3. Bacteria can be smaller than 1  $\mu\text{m}$  (Fröhlich-Nowoisky et al., 2016) and have also been observed at sizes  $<1\text{ }\mu\text{m}$  in a laboratory study with a WIBS (Hernandez et al., 2016). However, the strength of the fluorescence depends on the size of a particle, with larger particles showing higher intensity (**Figure 7g–i**) since they can contain more fluorophores (Savage et al., 2017). **Figure 7d–f** shows that  $HFA_A$  concentrations were highest at sizes  $<1\text{ }\mu\text{m}$ . Thus, PBAPs might also contribute to the type A aerosols at smaller sizes.

The environmental conditions in period 2 promote the sources and mechanisms involved in PBAP production and support our findings. The highest  $f_{HFA}$  values from the entire campaign during June and July coincided with peak solar radiation and seawater Chl-a concentration, indicating increased marine biological activity in the study area (**Figures 2 and 3c**). Solar radiation enhances marine biological activity, including phytoplankton blooms and subsequent bacterial growth (Niebauer, 1991; Perrette et al., 2011). This is consistent with the larger numbers of bacteria and phytoplankton cells observed in surface waters in the summer of 2020 compared to the rest of the drift (Figure S15a and b). Phytoplankton blooms with associated elevated bacterial counts in the Arctic can lead to enhanced aerosolization of cells (Feltracco et al., 2021). Moreover, long-range transport of aerosols from lower latitudes into the Arctic is limited during summer

(Schmale et al., 2011; Willis et al., 2018), and the primary source of aerosols becomes the central Arctic itself (Stohl, 2006). Period 2 starts after the Arctic haze (period 1) has vanished, and less anthropogenic influence is supported by the lower correlation between eBC and  $N_{HFA}$ , as depicted in **Figure 5**. These conditions suggest that HFA in period 2 could be influenced by local, marine sources. This is in agreement with findings from Kawana et al. (2024), who found positive correlations between marine aerosol sources and FA in the Bering Sea and the Arctic Ocean. In contrast, Perring et al. (2023) conducted the measurements of biological FA from an airplane over the ocean and sea ice around Utqiagvik in Alaska and observed no relationship between ocean biological activity and HFA. Using back trajectories, they attributed the FA to terrestrial sources. This finding differs from ours, as it appears that our measurements are more strongly influenced by marine sources. A potential reason for the different findings could be the difference in sampling altitude. The atmospheric boundary layer in the Arctic can be strongly stratified; hence, aerosol composition and sources can change with altitude. It might also be an indication that the fluorescence signal from terrestrial sources is stronger than that of marine sources, as Perring et al. (2023) see overall higher FA concentrations than we do. Our measurements were most of the time conducted further away from terrestrial sources than in Perring et al. (2023); hence, we might have captured more specifically marine signatures, which otherwise might have been overwhelmed by terrestrial sources. From Figure S7, we see that the air masses in our study were most influenced by open ocean and ice. However, occasional small contributions from land surfaces cannot be ruled out, as depicted in Figure S7.

Despite the similar type contributions to periods 2 and 3 (dominant types A and AB, Figure S5), the size distributions of HFA in period 3 (**Figure 7c, f, and i**) do not show a mode between 2 and 3  $\mu\text{m}$ . Instead, there is a mode  $<1\text{ }\mu\text{m}$  of HFA concentrations of type AB and a mode around 1  $\mu\text{m}$  of  $f_{HFA}$  of types A and AB. This suggests that period 3 had a different biological source of aerosols, that is, biological material that differs from period 2, but that is detected as types A and AB. This is potentially caused by seasonality in biological production. Period 3 occurred during fall with minimal solar radiation and the freeze-up in progress. According to **Figure 1**, *RV Polarstern* was located in the northern part of the Laptev Sea, approximately 320 km from the ice edge on October 1, 2019, and this distance increased to about 1,000 km by the end of the month due to the ongoing freezing process (Krumpfen et al., 2021). Air masses during period 3 came mainly from the open Laptev Sea (Figure S16). Also, Chl-a measurements show elevated concentrations (up to  $0.75\text{ }\mu\text{g}\text{L}^{-1}$ ) in November during MOSAiC (Figure S4) compared to later in the season, indicating the previous occurrence of a fall bloom. The Laptev Sea receives nutrient inputs from rivers in Siberia, which can enhance net primary production of biomass (Terhaar et al., 2021), especially if enhanced vertical mixing in fall transports these nutrients to the surface. Ardyna et al. (2014) found that

fall phytoplankton blooms increased by 70% between 2007 and 2012 in this region, compared to the period between 1998 and 2001. This means that the emission and transport of biological particles from previous fall blooms lasting through November in the region could be responsible for our observations of type A fluorescence particles during period 3.

In addition to explaining elevated FA concentrations, timing and strong seasonality in biological production could explain the differences in observed size distributions based on the type of phytoplankton communities and the presence of bacteria. While larger phytoplankton species are known to dominate Arctic blooms, small phytoplankton can be more efficient in thriving in nutrient- and light-limited conditions and thus may survive longer in the fall and dominate beyond the productive bloom phase in the high Arctic summer (Raven, 1998; Vader et al., 2015). Piwosz et al. (2013) discovered picoeukaryotes (1–3- $\mu\text{m}$  sized eukaryotic phytoplankton) in Arctic first-year ice and confirmed their ability to survive in the winter in sea ice. Moreover and perhaps more likely, given the fall bloom was already decaying during period 3, bacteria, which are also in the size range of 1  $\mu\text{m}$  (Fröhlich-Nowoisky et al., 2016), are expected to be present in higher relative proportions given they consume the phototrophic biomass independent of light availability. Despite lower total counts of bacteria and phytoplankton compared to period 2, the ratio of smaller bacteria to larger phytoplankton cells during period 3 is 2 orders of magnitude higher than during summer (Figure S15c). Hence, a shift from phytoplankton to bacterial cells could explain the observed size distributions. Note that we observe a relative enrichment around 1  $\mu\text{m}$  in the fraction of HFA particles of types A and AB during period 3 on top of an elevated absolute concentration of HFA at this size compared to period 2 (Figure 7). This discussion highlights the challenge of attributing specific sources to HFA types, and more detailed information about the composition of the HFA is necessary to conclude their sources. However, it can be concluded that different types and sizes of HFA, and likely PBAP, are present at other times of the year, indicating different source types.

### 3.6. HFA and warm INP

Several studies have indicated that PBAP are prominent INPs at warmer temperatures, typically above  $-10^{\circ}\text{C}$  (Després et al., 2012; Hartmann et al., 2020; Huang et al., 2021). Irish et al. (2017) found INPs activated at temperatures as high as  $-14^{\circ}\text{C}$  in Canadian Arctic seawater and SML and associated the INP activity with biological microorganisms. In a recent study, Kawana et al. (2024) demonstrated that INPs were best correlated with FA of types AB and ABC in samples collected over the North Pacific Ocean, the Bering Sea, and the Arctic Ocean in the autumn of 2019. The authors attributed types AB and ABC in FA to marine biogenic sources. Hence, the INP observations from MOSAiC can provide additional evidence supporting the association of observed HFA types with marine PBAP. Freitas et al. (2023) also found PBAP concentrations related to INP concentrations above  $-15^{\circ}\text{C}$  in Ny-Ålesund.

They identified PBAPs at an emission wavelength corresponding to type A HFA of the WIBS-NEO.

The monthly average number concentration of INP freezing at temperatures above  $-9^{\circ}\text{C}$  (warm INPs) appears to exhibit a covariation with  $f_{\text{HFA}}$  of types A and AB, as depicted in Figure 3d. Figure 8 shows the average  $f_{\text{HFA}}$  and fluorescence type composition of HFA for samples collected on days when the warmest INPs detected were at temperatures above  $-9^{\circ}\text{C}$ , between  $-9^{\circ}\text{C}$  and  $-15^{\circ}\text{C}$ , and below  $-15^{\circ}\text{C}$ . Aerosol samples collected with warm INPs ( $\geq 9^{\circ}\text{C}$ ) had an  $f_{\text{HFA}}$  approximately 7.5 times larger than the average  $f_{\text{HFA}}$  for samples collected with colder INPs ( $< -15^{\circ}\text{C}$ ). Moreover, the fluorescence types of HFA associated with warmer INP samples were dominated by types A and AB, whereby these types only play a minor role for samples associated with colder INP. The data corresponding to the warmer than  $-9^{\circ}\text{C}$  bin primarily came from period 2, while the other colder 2 sample bins included data from both periods 1 and 2. This further strengthens the hypothesis that HFA of types A and AB is likely related to PBAP.

We only find a covariance of  $f_{\text{HFA}}$  with warm INP but not with  $N_{\text{HFA}}$  directly. For example,  $N_{\text{HFA}}$  are approximately 3 times more abundant in May than in June (Figure S3), where roughly a factor of 10 higher warm INP concentrations are found in June (Figure 3d). Therefore, our observations can only use warm INP abundance as a surrogate for the presence of biological particles rather than establishing a quantitative relationship between FA and INP abundance. However, the covariance between  $f_{\text{HFA}}$  and warm INP does not seem to be a coincidence since similar observations were made over the Southern Ocean (Figure S17). Unfortunately, the potential reasons for this still inconclusive behavior cannot be revealed here because this would require more detailed measurements of the nature of PBAP and warm INPs. For example, it is conceivable that WIBS type A measurements in May and June cannot distinguish between PBAP, which have significantly different ice nucleating abilities.

### 3.7. Potential emission mechanisms in the central Arctic Ocean

While we explained the nature of sources previously, we focus here on potential release mechanisms. Given that  $f_{\text{HFA}}$  decreases with increasing wind speed (Figure 6), but strong biological contribution (as approximated by type A presence) occurs mainly during high  $f_{\text{HFA}}$  days (Figure 4), the investigation of the HFA release mechanisms under low wind conditions is necessary.

FA may be generated from bubbles bursting under low wind speeds. Bubbles can form even without high wind speed in leads in the central Arctic Ocean (Norris et al., 2011). Potential mechanisms such as bubble nucleation from the mixing of cold and warm water, resulting in decreased gas solubility, respiration by algae and phytoplankton populations, or the release of bubbles trapped in melting ice. Another potential source of bubbles is described by Fernández-Méndez et al. (2014), who found oxygenated bubbles produced by algae during

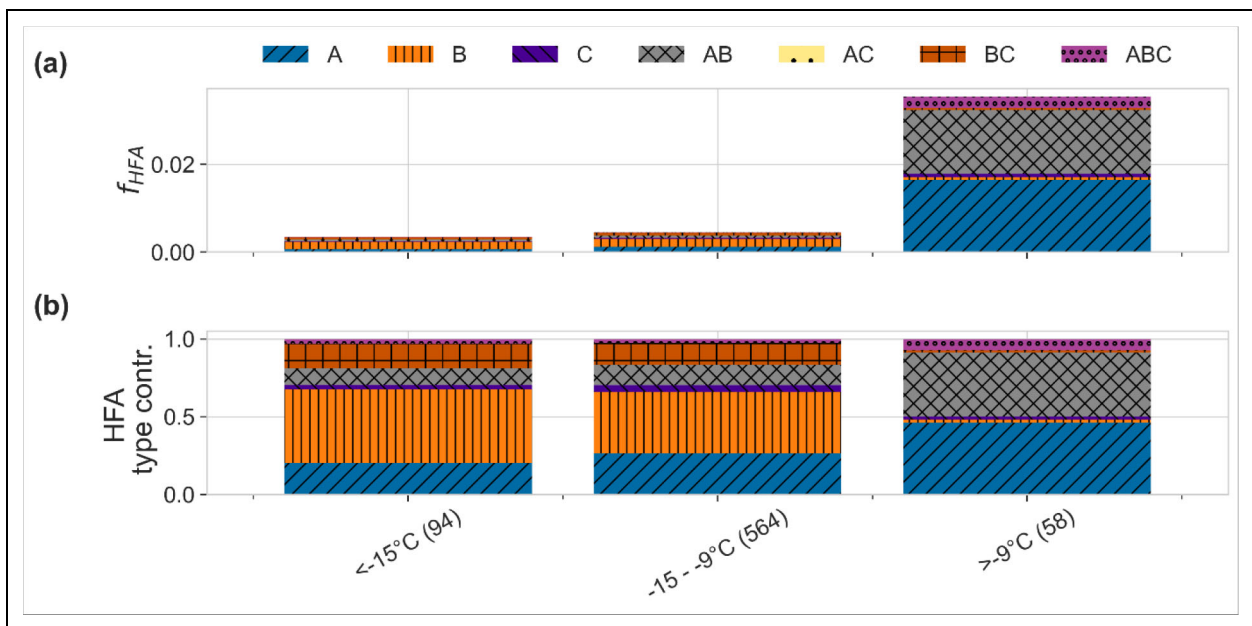


**Figure 8. Fluorescence type contributions to ice nucleating particles (INPs).** Comparison of the absolute hyperfluorescent aerosol (HFA) fractions ( $f_{HFA}$ ), split into different fluorescence types (a) and relative type contributions to the HFA (b) during the Multidisciplinary drifting Observatory for the Study of Arctic Climate (MOSAiC) Expedition at 3 different INP temperature regimes: for days where the warmest observed INPs were colder than  $-15^{\circ}\text{C}$ , where they were between  $-15^{\circ}\text{C}$  and  $-9^{\circ}\text{C}$ , and where INPs warmer than  $-9^{\circ}\text{C}$  were observed. The numbers in the parenthesis represent the number of hourly average HFA data points within each bin. The different fluorescent particle types are explained in **Table 1** in Section 2.3.

photosynthesis. This process depends on light and is therefore limited to the period between March and September.

The release of PBAPs via bubble bursting requires areas where (i) water and air are in direct contact and (ii) microbial organisms are present. During MOSAiC, period 2 exhibited such conditions (Figure S18). It featured the largest melt-pond fraction (Webster et al., 2022), and, starting from the beginning of June, the ship frequently encountered large areas of open water and leads. Melt ponds form on the surface of sea ice due to melting snow and ice (Webster et al., 2022). They can consist of either freshwater or a mixture of fresh and salty water if the pond's base is connected to the underlying seawater (Hornier et al., 1992; Kramer and Kiko, 2011). Melt ponds contain microorganisms like microalgae or bacteria (Sørensen et al., 2017) and can be the hot spots of biological activity (Hancke et al., 2022). Melt ponds have been suggested to potentially influence the atmospheric aerosol properties, particularly that of INPs (Creamean et al., 2022). However, the mechanisms by which microorganisms from melt ponds are transported into the atmosphere are not yet well understood. As discussed above, it can be speculated that bubble bursting, even in the absence of high winds, could release aerosols from melt ponds.

Freshwater from melting snow can form thin layers on the seawater surface in leads. The interface between the meltwater layer and seawater may contain a high biomass layer, as Smith et al. (2023) observed during the MOSAiC expedition. This biomass could contribute to PBAP being ejected into the atmosphere during bubble bursting. However, biomass in the meltwater layer itself can be low

because microorganisms from seawater are not well adapted to the freshwater (Mirrieles et al., 2022; Smith et al., 2023). Consequently, the meltwater layer is believed to impede the exchange between the ocean and the atmosphere, including the emission of PBAP (Smith et al., 2023). However, as meltwater layers form only for specific periods in some of the lead systems (Salganik et al., 2023), direct emission of FA into the atmosphere from high biomass water may still occur in some lead systems, for example, during mixing events (Smith et al., 2023).

These findings highlight the complexity of processes occurring at the ocean–atmosphere interface during summer, and further investigations are necessary to understand the release mechanisms and the significance of melt ponds, meltwater layers, and open leads as a source of atmospheric PBAP and INP in the central Arctic Ocean.

#### 4. Conclusions

We presented the annual cycle (October 2019–September 2020) of FA and HFA from the data collected with the WIBS during the MOSAiC expedition in the central Arctic Ocean. We assessed various properties of FA and HFA, including number concentrations and fluorescence types, throughout the year and used ancillary measurements from the same expedition to investigate potential sources and release mechanisms of FA. The strong annual cycles in HFA suggest that they do not represent a constant fraction of total atmospheric aerosols through the year but vary as a function of emission sources and transport patterns. We found 3 distinct periods. Period 1 (November 2019–April 2020 and September 2020) was characterized by relatively



high  $N_{\text{HFA}}$ , low  $f_{\text{HFA}}$ , and the dominance of type B, mostly linked to Arctic haze. Interestingly, there were distinct bursts of several hours length with high- $f_{\text{HFA}}$ . Period 2 (May 2020–August 2020) is characterized by relatively low median  $N_{\text{HFA}}$ , high median  $f_{\text{HFA}}$ , and the dominance of types A and AB, pointing toward significant biological contributions. Period 3 (October–November 2019) stands out due to high  $f_{\text{HFA}}$  dominated by types A and AB in combination with the absence of solar radiation and ongoing freeze-up. Our study shows that the WIBS is sensitive to anthropogenic aerosol sources, which likely affect fluorescence types B and BC, as evidenced by the correlation of eBC with these types, particularly in period 1. HFA of types A, AB, and ABC were associated with biological sources and are present throughout the year in the Arctic lower atmosphere. This notably includes the dark winter months, where such particles were present during 5 specific events. These findings point toward the presence of airborne microbial organisms in the Arctic winter. They could be emitted directly from the water, ice or snow, or originate from sublimating ice crystals during precipitation. These hypotheses warrant further investigations.

In summer as well as autumn, marine microbial activity is likely responsible for higher fractions of HFA and their strong relationship to INPs freezing at warm temperatures ( $-9^{\circ}\text{C}$ ). Interestingly, we observed a dominant mode of the HFA size distribution ( $2-3\ \mu\text{m}$ ) in summer and a smaller mode in autumn, concurring with the usual succession in Arctic marine microbiological communities. We suggest that bubble bursting at low-wind conditions could promote high  $f_{\text{HFA}}$  under the low-wind conditions characteristic for summer.

In winter, the typical high wind speed conditions lead to higher absolute FA and HFA concentrations, but to smaller fractions of fluorescent particles, indicating that wind does not enrich but rather dilutes the fractional contribution of fluorescent particles. Moreover, the type composition of FA and HFA during blowing snow conditions is not significantly different from nonblowing snow conditions during period 1 (dominant type B), which might indicate that previously deposited airborne particles are resuspended.

While our study suggests several potential seasonal source mechanisms of HFA, the exact processes remain to be revealed and require targeted field studies including the measurements of specific tracers for airborne biological and fluorescent particles. For example, the measurements of FA could be made on-site with sampled water from leads or melt ponds in a bubble chamber, or even directly above the water surface in floating chambers, together with analyses (e.g., DNA sequencing) of the microorganisms contained therein. Additional simultaneous measurements of the composition of microorganisms in the ice, snow, and SML and vertically resolved throughout the lower atmosphere would provide insight into which of the microorganisms are exchanged locally and which might be transported over long distances. This could be used to establish a mechanistic link between individual marine microorganisms and FA. Combining this detailed analysis with INP measurements bears a high

potential to narrow down the sources of local central Arctic INP.

In light of rapid climate change in the Arctic and its impact on sea ice, melt ponds, biological activity, and other factors relevant to Arctic PBAP, it is indispensable to shed further light on the nature and sources of these particles that can strongly influence the sensitive and important Arctic low-level mixed-phase cloud regime.

### Data accessibility statement

The following data sets were used for this manuscript:

- Beck et al. (2023). Wideband integrated bioaerosol sensor (WIBS) excited, fluorescent, and hyper-fluorescent particle number concentrations and normalized size distributions ( $\text{dN}/\text{dlogDp}$ ) measured in the Swiss container during MOSAiC 2019/2020. PANGAEA. DOI: <https://doi.org/10.1594/PANGAEA.961065>.
- Heutte et al. (2022). Equivalent black carbon concentration in 10 minutes time resolution, measured in the Swiss container during MOSAiC 2019/2020. PANGAEA. DOI: <https://doi.org/10.1594/PANGAEA.952251>.
- Beck et al. (2022b). Pollution mask for the continuous corrected particle number concentration data in 1 min resolution, measured in the Swiss aerosol container during MOSAiC 2019/2020. PANGAEA. DOI: <https://doi.org/10.1594/PANGAEA.941335>.
- Schmithuesen (2021a). Continuous meteorological surface measurement during POLARSTERN cruise PS122/1, Alfred Wegener Institute, Helmholtz Centre for Polar and Marine Research, Bremerhaven. PANGAEA. DOI: <https://doi.org/10.1594/PANGAEA.935221>.
- Schmithuesen (2021b). Continuous meteorological surface measurement during POLARSTERN cruise PS122/2, Alfred Wegener Institute, Helmholtz Centre for Polar and Marine Research, Bremerhaven. PANGAEA. DOI: <https://doi.org/10.1594/PANGAEA.935222>.
- Schmithuesen (2021c). Continuous meteorological surface measurement during POLARSTERN cruise PS122/3, Alfred Wegener Institute, Helmholtz Centre for Polar and Marine Research, Bremerhaven. PANGAEA. DOI: <https://doi.org/10.1594/PANGAEA.935223>.
- Schmithuesen (2021d). Continuous meteorological surface measurement during POLARSTERN cruise PS122/4, Alfred Wegener Institute, Helmholtz Centre for Polar and Marine Research, Bremerhaven. PANGAEA. DOI: <https://doi.org/10.1594/PANGAEA.935224>.
- Schmithuesen (2021e). Continuous meteorological surface measurement during POLARSTERN cruise PS122/5, Alfred Wegener Institute, Helmholtz Centre for Polar and Marine Research, Bremerhaven. PANGAEA. DOI: <https://doi.org/10.1594/PANGAEA.935225>.

- Frey et al. (2023). Atmospheric snow particle flux in the Central Arctic during MOSAiC 2019-20. NERC EDS UK Polar Data Centre. DOI: <https://doi.org/10.5285/7D8E401B-2C75-4EE4-A753-C24B7E91E6E9>.
- Angot et al. (2022a). Carbon dioxide dry air mole fractions measured in the Swiss container during MOSAiC 2019/2020. PANGAEA. DOI: <https://doi.org/10.1594/PANGAEA.944248>.
- Angot et al. (2022b). Carbon monoxide dry air mole fractions measured in the Swiss container during MOSAiC 2019/2020. PANGAEA. DOI: <https://doi.org/10.1594/PANGAEA.944264>.
- Angot et al. (2022c). Methane dry air mole fractions measured in the Swiss container during MOSAiC 2019/2020. PANGAEA. DOI: <https://doi.org/10.1594/PANGAEA.944258>.
- Tatzelt et al. (2020). Ice Nucleating Particle number concentration from low-volume sampling over the Southern Ocean during the austral summer of 2016/2017 on board the Antarctic Circumnavigation Expedition (ACE). Zenodo. DOI: <https://doi.org/10.5281/zenodo.4311665>.
- Moallemi et al. (2021). Number concentration and fluorescent class fraction of fluorescent and HFA particles measured during the Antarctic Circumnavigation Expedition. Zenodo. DOI: <https://doi.org/10.5281/zenodo.5109382>.
- Nicolaus et al. (2021). Visual panoramic photographs of the surface conditions during the MOSAiC campaign 2019/20. PANGAEA. DOI: <https://doi.org/10.1594/PANGAEA.938534>.
- Willmes et al. (2023). ArcLeads: Daily sea-ice lead maps for the Arctic, 2002-2021, NOV-APR. PANGAEA. DOI: <https://doi.org/10.1594/PANGAEA.955561>.
- Müller et al. (2023). Flow cytometry dataset from CTD casts showing the abundance of microorganisms (smaller than 20  $\mu\text{m}$ ) during the Arctic MOSAiC expedition. PANGAEA. DOI: <https://doi.org/10.1594/PANGAEA.963430>.

The INP data are available in the U.S. Department of Energy data archive under <https://doi.org/10.5439/1798162>. The melt pond data set can be downloaded from the University of Bremen website: <https://seaice.uni-bremen.de/melt-ponds/>. DRUM INP data are provided by the Department of Energy ARM user facility data discovery tool: <https://adc.arm.gov/discovery/#/results/iopShortName::amf2019inpMOSAIC2>. FLEXPART backward dispersion model simulations from MOSAiC are provided by the FLEXPART group at the University of Vienna and can be downloaded here: <https://img.univie.ac.at/webdata/mosaic>.

### Supplemental files

The supplemental files for this article can be found as follows:

The supplemental file (.docx) is split into the following sections:

**Section S1.** Local pollution detection

**Section S2.** Overview of the fluorescent aerosol characteristics and ancillary data throughout the expedition

**Section S3.** Event analysis

**Section S4.** Potential source contribution from wind driven processes to fluorescent aerosols

**Section S5.** Fluorescence mapping

**Section S6.** Biological influence on fluorescent aerosols and their particle size distributions

**Section S7.** Relation of  $f_{\text{HFA}}$  and INPs

**Section S8.** Summer sea ice conditions

### Acknowledgments

The authors thank the land-based MOSAiC teams of the University of Helsinki and the Paul Scherrer Institute for their incessant support. The authors would like to thank the *RV Polarstern* crew and in particular the workshops for their fantastic support. They thank all those who contributed to MOSAiC and made this endeavor possible (Nixdorf et al., 2021). L. Wischniewski, E. Chamberlain, T. Brenneis, and A. Terbrüggen are acknowledged for help with the Chl-a analyses. Elina Viinamäki prepared the Bacteria cultures for the bubble tank experiment. They further thank the team of technicians, which supported the measurements and aerosol sampling in the U.S. Department of Energy (DOE) AOS container during the MOSAiC campaign. Trajectory analysis from the FLEXPART model simulations, performed by the FLEXPART group at the University of Vienna. Rachel M. Kirpes is acknowledged for leading University of Michigan impactor sampling preparations.

### Funding

Data used in this manuscript were produced as part of the international Multidisciplinary drifting Observatory for the Study of the Arctic Climate (MOSAIC) with the tag MOSAiC20192020 and the project\_ID: AWI\_PS122\_00. This work was financed by the Swiss National Science Foundation (grant no. 200021\_188478) and Swiss Polar Institute (grant no. DIRCR-2018-004). TJ received funding from the Academy of Finland (334514) and acknowledges EMME-CARE, funded by the European Union's Horizon 2020 research and innovation program under grant agreement No. 856612 and the Cyprus Government. LQ thanks the European Research Council ERC (GASPARCON—grant no. 714621). JC was funded by the DOE ARM and Atmospheric System Research (ASR) programs (DE-AC05-76RL01830, DE-SC0019745, and DE-SC0022046). JAM and KAP were supported by the DOE ARM, ASR, and Early Career programs (DE-SC0019172 and DE-SC0022046), and HEK was supported by fellowships from the University of Michigan Arctic Internship Fellowship and a College of Literature, Science, and the Arts Internship Fellowship. We further received funding from the U.S. Department of Energy Atmospheric System Research program grant no. DE-SC0022046 and DE-SC0019251. MMF was supported by the U.K. Natural Environment Research Council (NERC) (NE/S00257X/1) and the NERC National Capability International grant SURface FluxEs In AnTartica (SURFEIT) (NE/X009319/1). BH and NB were supported by the

European Union's Horizon 2020 research and innovation programme under grant agreement No 101003826 via project CRiceS (Climate Relevant interactions and feedbacks: the key role of sea ice and Snow in the polar and global climate system). JBP received funding from the Swiss Data Science Center Project (C20-01: ArcticNAP). CT was supported by the Deutsche Forschungsgemeinschaft (DFG) in the framework of the priority programme "Antarctic Research with comparative investigations in the Arctic sea ice areas" (SPP 1158 [grant no. STR 453/12-1]). This work was also supported by the Swedish Research Council (VR starting grant, 2018-05045). Parts of this research have been supported by the DFG SPP 1158, grant number 424326801. JS holds the Ingvar Kamprad Chair for Extreme Environments Research sponsored by Ferring Pharmaceuticals.

### Competing interests

The authors do not declare any competing interests.

### Author contributions

- Contributed to conception and design: JS, AM, IB.
- Contributed to acquisition of data: LLJQ, IB, JS, TJ, TL, JC, CJMH, OM, MMF, GF, JZ, MS, PZ, SH, CT, JAM, HEK, APA, KAP.
- Contributed to analysis and interpretation of data: All authors.
- Written the article: IB, AM, JS.
- Revised the article: All authors.
- Approved the submitted version for publication: All authors.

### References

- Abbatt, JPD, Leaitch, WR, Aliabadi, AA, Bertram, AK, Blanchet, J-P, Boivin-Rioux, A, Bozem, H, Burkart, J, Chang, RYW, Charette, J, Chaubey, JP, Christensen, RJ, Cirisan, A, Collins, DB, Croft, B, Dionne, J, Evans, GJ, Fletcher, CG, Galí, M, Ghahremaninezhad, R, Girard, E, Gong, W, Gosselin, M, Gourdal, M, Hanna, SJ, Hayashida, H, Herber, AB, Hesaraki, S, Hoor, P, Huang, L, Husherr, R, Irish, VE, Keita, SA, Kodros, JK, Köllner, F, Kolonjari, F, Kunkel, D, Ladino, LA, Law, K, Lévassieur, M, Libois, Q, Liggio, J, Lizotte, M, Macdonald, KM, Mahmood, R, Martin, RV, Mason, RH, Miller, LA, Moravek, A, Mortenson, E, Mungall, EL, Murphy, JG, Namazi, M, Norman, A-L, O'Neill, NT, Pierce, JR, Russell, LM, Schneider, J, Schulz, H, Sharma, S, Si, M, Staebler, RM, Steiner, NS, Thomas, JL, von Salzen, K, Wentzell, JJB, Willis, MD, Wentworth, GR, Xu, J-W, Yakobi-Hancock, JD.** 2019. Overview paper: New insights into aerosol and climate in the Arctic. *Atmospheric Chemistry and Physics* **19**(4): 2527–2560. DOI: <http://dx.doi.org/10.5194/acp-19-2527-2019>.
- Albrecht, BA.** 1989. Aerosols, cloud microphysics, and fractional cloudiness. *Science* **245**(4923): 1227–1230. DOI: <http://dx.doi.org/10.1126/science.245.4923.1227>.
- Angot, H, Beck, I, Jokinen, T, Laurila, T, Quéléver, L, Schmale, J.** 2022a. Carbon dioxide dry air mole fractions measured in the Swiss container during MOSAiC 2019/2020 [dataset]. PANGAEA. DOI: <https://doi.org/10.1594/PANGAEA.944248>.
- Angot, H, Beck, I, Jokinen, T, Laurila, T, Quéléver, L, Schmale, J.** 2022b. Carbon monoxide dry air mole fractions measured in the Swiss container during MOSAiC 2019/2020 [dataset]. PANGAEA. DOI: <https://doi.org/10.1594/PANGAEA.944264>.
- Angot, H, Beck, I, Jokinen, T, Laurila, T, Quéléver, L, Schmale, J.** 2022c. Methane dry air mole fractions measured in the Swiss container during MOSAiC 2019/2020 [dataset]. PANGAEA. DOI: <https://doi.org/10.1594/PANGAEA.944258>.
- Angot, H, Blomquist, B, Howard, D, Archer, S, Bariteau, L, Beck, I, Boyer, M, Crotwell, M, Helmig, D, Hueber, J, Jacobi, H-W, Jokinen, T, Kulmala, M, Lan, X, Laurila, T, Madronich, M, Neff, D, Petäjä, T, Posman, K, Quéléver, L, Shupe, MD, Vimont, I, Schmale, J.** 2022d. Year-round trace gas measurements in the central Arctic during the MOSAiC expedition. *Scientific Data* **9**: 723. DOI: <http://dx.doi.org/10.1038/s41597-022-01769-6>.
- Ardyna, M, Babin, M, Gosselin, M, Devred, E, Rainville, L, Tremblay, J-É.** 2014. Recent Arctic Ocean Sea ice loss triggers novel fall phytoplankton blooms. *Geophysical Research Letters* **41**(17): 6207–6212. DOI: <http://dx.doi.org/10.1002/2014GL061047>.
- Arrigo, KR, Van Dijken, GL.** 2015. Continued increases in Arctic Ocean primary production. *Progress in Oceanography* **136**: 60–70. DOI: <http://dx.doi.org/10.1016/j.pocean.2015.05.002>.
- Barrett, TE, Sheesley, RJ.** 2017. Year-round optical properties and source characterization of Arctic organic carbon aerosols on the North Slope Alaska. *Journal of Geophysical Research: Atmospheres* **122**(17): 9319–9331. DOI: <http://dx.doi.org/10.1002/2016JD026194>.
- Barrie, LA.** 1986. Arctic air pollution: An overview of current knowledge. *Atmospheric Environment (1967)* **20**(4): 643–663. DOI: [http://dx.doi.org/10.1016/0004-6981\(86\)90180-0](http://dx.doi.org/10.1016/0004-6981(86)90180-0).
- Barrie, LA, Hoff, RM, Daggupaty, SM.** 1981. The influence of mid-latitude pollution sources on haze in the Canadian Arctic. *Atmospheric Environment (1967)* **15**(8): 1407–1419. DOI: [http://dx.doi.org/10.1016/0004-6981\(81\)90347-4](http://dx.doi.org/10.1016/0004-6981(81)90347-4).
- Beck, I, Angot, H, Baccharini, A, Dada, L, Quéléver, L, Jokinen, T, Laurila, T, Lampimäki, M, Bukowiecki, N, Boyer, M, Gong, X, Gysel-Beer, M, Petäjä, T, Wang, J, Schmale, J.** 2022a. Automated identification of local contamination in remote atmospheric composition time series. *Atmospheric Measurement Techniques* **15**(14): 4195–4224. DOI: <http://dx.doi.org/10.5194/amt-15-4195-2022>.
- Beck, I, Moallemi, A, Rolo, M, Quéléver, L, Jokinen, T, Laurila, T, Schmale, J.** 2023. Wideband integrated bioaerosol sensor (WIBS) excited, fluorescent, and hyper-fluorescent particle number concentrations

- and normalized size distributions (dN/dlogDp) measured in the Swiss container during MOSAiC 2019/2020. PANGAEA. DOI: <http://dx.doi.org/10.1594/PANGAEA.961065>.
- Beck, I, Quéléver, L, Laurila, T, Jokinen, T, Baccarini, A, Angot, H, Schmale, J.** 2022b. Pollution mask for the continuous corrected particle number concentration data in 1 min resolution, measured in the Swiss aerosol container during MOSAiC 2019/2020. PANGAEA. DOI: <http://dx.doi.org/10.1594/PANGAEA.941335>.
- Berge, J, Daase, M, Renaud, PE, Ambrose, WG, Darnis, G, Last, KS, Leu, E, Cohen, JH, Johnsen, G, Moline, MA, Cottier, F, Varpe, Ø, Shunatova, N, Bałazy, P, Morata, N, Massabuau, J-C, Falk-Petersen, S, Kosobokova, K, Hoppe, CJM, Węśławski, JM, Kukliński, P, Legeżyńska, J, Nikishina, D, Cusa, M, Kędra, M, Włodarska-Kowalczyk, M, Vogedes, D, Camus, L, Tran, D, Michaud, E, Gabrielsen, TM, Granovitch, A, Gonchar, A, Krapp, R, Callesen, TA.** 2015. Unexpected levels of biological activity during the polar night offer new perspectives on a warming Arctic. *Current Biology* **25**: 2555–2561. DOI: <http://dx.doi.org/10.1016/j.cub.2015.08.024>.
- Bigg, EK, Leck, C.** 2008. The composition of fragments of bubbles bursting at the ocean surface. *Journal of Geophysical Research: Atmospheres* **113**(D11). DOI: <http://dx.doi.org/10.1029/2007JD009078>.
- Blanchard, DC.** 1989. The ejection of drops from the sea and their enrichment with bacteria and other materials: A review. *Estuaries* **12**: 127–137. DOI: <http://dx.doi.org/10.2307/1351816>.
- Bond, TC, Doherty, SJ, Fahey, DW, Forster, PM, Berntsen, T, DeAngelo, BJ, Flanner, MG, Ghan, S, Kärcher, B, Koch, D, Kinne, S, Kondo, Y, Quinn, PK, Sarofim, MC, Schultz, MG, Schulz, M, Venkataraman, C, Zhang, H, Zhang, S, Bellouin, N, Guttikunda, SK, Hopke, PK, Jacobson, MZ, Kaiser, JW, Klimont, Z, Lohmann, U, Schwarz, JP, Shindell, D, Storelvmo, T, Warren, SG, Zender, CS.** 2013. Bounding the role of black carbon in the climate system: A scientific assessment. *Journal of Geophysical Research: Atmospheres* **118**(11): 5380–5552. DOI: <http://dx.doi.org/10.1002/jgrd.50171>.
- Boyer, M, Aliaga, D, Pernov, JB, Angot, H, Quéléver, LLJ, Dada, L, Heutte, B, Dall'Osto, M, Beddows, DCS, Brasseur, Z, Beck, I, Bucci, S, Duetsch, M, Stohl, A, Laurila, T, Asmi, E, Massling, A, Thomas, DC, Nøjgaard, JK, Chan, T, Sharma, S, Tunved, P, Krejci, R, Hansson, HC, Bianchi, F, Lehtipalo, K, Wiedensohler, A, Weinhold, K, Kulmala, M, Petäjä, T, Sipilä, M, Schmale, J, Jokinen, T.** 2023. A full year of aerosol size distribution data from the central Arctic under an extreme positive Arctic Oscillation: Insights from the Multidisciplinary drifting Observatory for the Study of Arctic climate (MOSAiC) expedition. *Atmospheric Chemistry and Physics* **23**(1) 389–415. DOI: <http://dx.doi.org/10.5194/acp-23-389-2023>.
- Burrows, SM, Easter, RC, Liu, X, Ma, P-L, Wang, H, Elliott, SM, Singh, B, Zhang, K, Rasch, PJ.** 2022. OCEANFILMS (Organic Compounds from Ecosystems to Aerosols: Natural Films and Interfaces via Langmuir Molecular Surfactants) sea spray organic aerosol emissions—Implementation in a global climate model and impacts on clouds. *Atmospheric Chemistry and Physics* **22**(8): 5223–5251. DOI: <http://dx.doi.org/10.5194/acp-22-5223-2022>.
- Campbell, ID, McDonald, K, Flannigan, MD, Krin-gayark, J.** 1999. Long-distance transport of pollen into the Arctic. *Nature* **399**: 29–30. DOI: <http://dx.doi.org/10.1038/19891>.
- Chen, Q, Mirrieles, JA, Thanekar, S, Loeb, NA, Kirpes, RM, Upchurch, LM, Barget, AJ, Lata, NN, Raso, ARW, McNamara, SM, China, S, Quinn, PK, Ault, AP, Kennedy, A, Shepson, PB, Fuentes, JD, Pratt, KA.** 2022. Atmospheric particle abundance and sea salt aerosol observations in the springtime Arctic: A focus on blowing snow and leads. *Atmospheric Chemistry and Physics* **22**(23): 15263–15285. DOI: <http://dx.doi.org/10.5194/acp-22-15263-2022>.
- Crawford, I, Gallagher, MW, Bower, KN, Choularton, TW, Flynn, MJ, Ruske, S, Listowski, C, Brough, N, Lachlan-Cope, T, Fleming, ZL, Foot, VE, Stanley, WR.** 2017. Real-time detection of airborne fluorescent bioparticles in Antarctica. *Atmospheric Chemistry and Physics* **17**(23): 14291–14307. DOI: <http://dx.doi.org/10.5194/acp-17-14291-2017>.
- Creamean, JM.** 2021. *Size-resolved ice nucleating particle (INP) concentrations from the MOSAiC campaign.* USA: ORNL. DOI: <https://doi.org/10.5439/1798162>.
- Creamean, JM, Barry, K, Hill, TCJ, Hume, C, DeMott, PJ, Shupe, MD, Dahlke, S, Willmes, S, Schmale, J, Beck, I, Hoppe, CJM, Fong, A, Chamberlain, E, Bowman, J, Scharien, R, Persson, O.** 2022. Annual cycle observations of aerosols capable of ice formation in central Arctic clouds. *Nature Communications* **13**: 3537. DOI: <http://dx.doi.org/10.1038/s41467-022-31182-x>.
- Creamean, JM, Maahn, M, de Boer, G, McComiskey, A, Sedlacek, AJ, Feng, Y.** 2018. The influence of local oil exploration and regional wildfires on summer 2015 aerosol over the North Slope of Alaska. *Atmospheric Chemistry and Physics* **18**(2): 555–570. DOI: <http://dx.doi.org/10.5194/acp-18-555-2018>.
- Croft, B, Martin, RV, Leaitch, WR, Burkart, J, Chang, RY-W, Collins, DB, Hayes, PL, Hodshire, AL, Huang, L, Kodros, JK, Moravek, A, Mungall, EL, Murphy, JG, Sharma, S, Tremblay, S, Wentworth, GR, Willis, MD, Abbatt, JPD, Pierce, JR.** 2019. Arctic marine secondary organic aerosol contributes significantly to summertime particle size distributions in the Canadian Arctic Archipelago. *Atmospheric Chemistry and Physics* **19**(5): 2787–2812. DOI: <http://dx.doi.org/10.5194/acp-19-2787-2019>.
- Cuthbertson, L, Amores-Arrocha, H, Malard, LA, Els, N, Sattler, B, Pearce, DA.** 2017. Characterisation of Arctic bacterial communities in the air above

- Svalbard. *Biology* **6**(2): 29. DOI: <http://dx.doi.org/10.3390/biology6020029>.
- de Boer, G, Hashino, T, Tripoli, GJ, Eloranta, EW.** 2013. A numerical study of aerosol influence on mixed-phase stratiform clouds through modulation of the liquid phase. *Atmospheric Chemistry and Physics* **13**(4): 1733–1749. DOI: <http://dx.doi.org/10.5194/acp-13-1733-2013>.
- DeCarlo, PF, Kimmel, JR, Trimborn, A, Northway, MJ, Jayne, JT, Aiken, AC, Gonin, M, Fuhrer, K, Horvath, T, Docherty, KS, Worsnop, DR, Jimenez, JL.** 2006. Field-deployable, high-resolution, time-of-flight aerosol mass spectrometer. *Analytical Chemistry* **78**(24): 8281–8289. DOI: <http://dx.doi.org/10.1021/ac061249n>.
- Deepak, A, Vali, G** eds. 1992. *The International Global Aerosol Program (IGAP) plan*. Hampton, VA: A. Deepak.
- de Leeuw, G, Andreas, EL, Anguelova, MD, Fairall, CW, Lewis, ER, O'Dowd, C, Schulz, M, Schwartz, SE.** 2011. Production flux of sea spray aerosol. *Reviews of Geophysics* **49**(2). DOI: <http://dx.doi.org/10.1029/2010RG000349>.
- Després, VR, Huffman, JA, Burrows, SM, Hoose, C, Safatov, AS, Buryak, G, Fröhlich-Nowoisky, J, Elbert, W, Andreae, MO, Pöschl, U, Jaenicke, R.** 2012. Primary biological aerosol particles in the atmosphere: A review. *Tellus B: Chemical and Physical Meteorology* **64**: 15598. DOI: <http://dx.doi.org/10.3402/tellusb.v64i0.15598>.
- Eirund, GK, Possner, A, Lohmann, U.** 2019. Response of Arctic mixed-phase clouds to aerosol perturbations under different surface forcings. *Atmospheric Chemistry and Physics* **19**(15) 9847–9864. DOI: <http://dx.doi.org/10.5194/acp-19-9847-2019>.
- Feltracco, M, Barbaro, E, Hoppe, CJM, Wolf, KKE, Spolaor, A, Layton, R, Keuschnig, C, Barbante, C, Gambaro, A, Larose, C.** 2021. Airborne bacteria and particulate chemistry capture Phytoplankton bloom dynamics in an Arctic fjord. *Atmospheric Environment* **256**: 118458. DOI: <http://dx.doi.org/10.1016/j.atmosenv.2021.118458>.
- Fernández-Méndez, M, Olsen, LM, Kauko, HM, Meyer, A, Rösel, A, Merkouriadi, I, Mundy, CJ, Ehn, JK, Johansson, AM, Wagner, PM, Ervik, Å, Sorrell, BK, Duarte, P, Wold, A, Hop, H, Assmy, P.** 2018. Algal hot spots in a changing Arctic Ocean: Sea-ice ridges and the snow-ice interface. *Frontiers in Marine Science* **5**: 75.
- Fernández-Méndez, M, Wenzhöfer, F, Peeken, I, Sørensen, HL, Glud, RN, Boetius, A.** 2014. Composition, buoyancy regulation and fate of ice algal aggregates in the Central Arctic Ocean. *PLoS One* **9**: e107452. DOI: <http://dx.doi.org/10.1371/journal.pone.0107452>.
- Forde, E, Gallagher, M, Walker, M, Foot, V, Attwood, A, Granger, G, Sarda-Estève, R, Stanley, W, Kaye, P, Topping, D.** 2019. Intercomparison of multiple UV-LIF spectrometers using the aerosol challenge simulator. *Atmosphere* **10**: 797. DOI: <http://dx.doi.org/10.3390/atmos10120797>.
- Fox-Kemper, B, Hewitt, HT, Xiao, C, Aðalgeirsdóttir, G, Drijfhout, SS, Edwards, TL, Golledge, NR, Hemer, M, Kopp, RE, Krinner, G, Mix, A, Notz, D, Nowicki, S, Nurhati, IS, Ruiz, L, Sallée, J-B, Slangen, ABA, Yu, Y.** 2021. Ocean, cryosphere and sea level change, in Masson-Delmotte, V, Zhai, P, Pirani, A, Connors, SL, Péan, C, Berger, S, Caud, N, Chen, Y, Goldfarb, L, Gomis, MI, Huang, M, Leitzell, K, Lonnoy, E, Matthews, JBR, Maycock, TK, Waterfield, T, Yelekçi, O, Yu, R, Zhou, B eds. *Climate change 2021: The physical science basis. Contribution of Working Group I to the Sixth Assessment Report of the Intergovernmental Panel on Climate Change*. Cambridge, UK; New York: Cambridge University Press: 1211–1362. DOI: <http://dx.doi.org/10.1017/9781009157896.011>.
- Freitas, GP, Adachi, K, Conen, F, Heslin-Rees, D, Krejci, R, Tobo, Y, Yttri, KE, Zieger, P.** 2023. Regionally sourced bioaerosols drive high-temperature ice nucleating particles in the Arctic. *Nature Communications* **14**: 5997. DOI: <http://dx.doi.org/10.1038/s41467-023-41696-7>.
- Freitas, GP, Stolle, C, Kaye, PH, Stanley, W, Herlemann, DPR, Salter, ME, Zieger, P.** 2022. Emission of primary bioaerosol particles from Baltic seawater. *Environmental Science: Atmospheres*. DOI: <http://dx.doi.org/10.1039/D2EA00047D>.
- Frey, MM, Norris, SJ, Brooks, IM, Anderson, PS, Nishimura, K, Yang, X, Jones, AE, Nerentorp Mastro Monaco, MG, Jones, DH, Wolff, EW.** 2020. First direct observation of sea salt aerosol production from blowing snow above sea ice. *Atmospheric Chemistry and Physics* **20**: 2549–2578. DOI: <http://dx.doi.org/10.5194/acp-20-2549-2020>.
- Frey, MM, Wagner, D, Kirchgassner, A, Uttal, T, Shupe, M.** 2023. Atmospheric snow particle flux in the central Arctic during MOSAiC 2019-20 (Version 1.0). Cambridge, UK: NERC EDS UK Polar Data Centre. DOI: <http://dx.doi.org/10.5285/7D8E401B-2C75-4EE4-A753-C24B7E91E6E9>.
- Fröhlich-Nowoisky, J, Kampf, CJ, Weber, B, Huffman, JA, Pöhlker, C, Andreae, MO, Lang-Yona, N, Burrows, SM, Gunthe, SS, Elbert, W, Su, H, Hoor, P, Thines, E, Hoffmann, T, Després, VR, Pöschl, U.** 2016. Bioaerosols in the earth system: Climate, health, and ecosystem interactions. *Atmospheric Research* **182**: 346–376. DOI: <http://dx.doi.org/10.1016/j.atmosres.2016.07.018>.
- Fu, P, Kawamura, K, Chen, J, Qin, M, Ren, L, Sun, Y, Wang, Z, Barrie, LA, Tachibana, E, Ding, A, Yamashita, Y.** 2015. Fluorescent water-soluble organic aerosols in the High Arctic atmosphere. *Scientific Reports* **5**: 9845. DOI: <http://dx.doi.org/10.1038/srep09845>.
- Gabey, AM, Gallagher, MW, Whitehead, J, Dorsey, JR, Kaye, PH, Stanley, WR.** 2010. Measurements and comparison of primary biological aerosol above and below a tropical forest canopy using a dual channel

- fluorescence spectrometer. *Atmospheric Chemistry and Physics* **10**: 4453–4466. DOI: <http://dx.doi.org/10.5194/acp-10-4453-2010>.
- Gregory, D, Morris, D.** 1996. The sensitivity of climate simulations to the specification of mixed phase clouds. *Climate Dynamics* **12**: 641–651. DOI: <http://dx.doi.org/10.1007/BF00216271>.
- Haas, C.** 2020. Master track of POLARSTERN cruise PS122/2 in 1 sec resolution. Alfred Wegener Institute, Helmholtz Centre for Polar and Marine Research, Bremerhaven. DOI: <http://dx.doi.org/10.1594/PANGAEA.924672>.
- Halsall, CJ, Barrie, LA, Fellin, P, Muir, DCG, Billeck, BN, Lockhart, L, Rovinsky, FYa, Kononov, EYa, Pastukhov, B.** 1997. Spatial and temporal variation of polycyclic aromatic hydrocarbons in the Arctic atmosphere. *Environmental Science & Technology* **31**: 3593–3599. DOI: <http://dx.doi.org/10.1021/es970342d>.
- Hancke, K, Kristiansen, S, Lund-Hansen, LC.** 2022. Highly productive ice algal mats in Arctic melt ponds: Primary production and carbon turnover. *Frontiers in Marine Science* **9**: 841720. DOI: <http://dx.doi.org/10.3389/fmars.2022.841720>.
- Hartmann, M, Adachi, K, Eppers, O, Haas, C, Herber, A, Holzinger, R, Hünerbein, A, Jäkel, E, Jentsch, C, van Pinxteren, M, Wex, H, Willmes, S, Stratmann, F.** 2020. Wintertime airborne measurements of ice nucleating particles in the High Arctic: A hint to a marine, biogenic source for ice nucleating particles. *Geophysical Research Letters* **47**: e2020GL087770. DOI: <http://dx.doi.org/10.1029/2020GL087770>.
- Hernandez, M, Perring, AE, McCabe, K, Kok, G, Granger, G, Baumgardner, D.** 2016. Chamber catalogues of optical and fluorescent signatures distinguish bioaerosol classes. *Atmospheric Measurement Techniques* **9**: 3283–3292. DOI: <http://dx.doi.org/10.5194/amt-9-3283-2016>.
- Heutte, B, Beck, I, Quééléver, L, Jokinen, T, Laurila, T, Dada, L, Schmale, J.** 2022. Equivalent black carbon concentration in 10 minutes time resolution, measured in the Swiss container during MOSAiC 2019/2020. PANGAEA. DOI: <http://dx.doi.org/10.1594/PANGAEA.952251>.
- Heutte, B, Bergner, N, Beck, I, Angot, H, Dada, L, Quééléver, LLJ, Laurila, T, Boyer, M, Bresseur, Z, Daelenbach, KR, Henning, S, Kuang, C, Kulmala, M, Lampilahti, J, Lampimäki, M, Petäjä, T, Shupe, MD, Sipilä, M, Uin, J, Jokinen, T, Schmale, J.** 2023. Measurements of aerosol microphysical and chemical properties in the central Arctic atmosphere during MOSAiC. *Scientific Data* **10**: 690. DOI: <http://dx.doi.org/10.1038/s41597-023-02586-1>.
- Hoose, C, Möhler, O.** 2012. Heterogeneous ice nucleation on atmospheric aerosols: A review of results from laboratory experiments. *Atmospheric Chemistry and Physics* **12**: 9817–9854. DOI: <http://dx.doi.org/10.5194/acp-12-9817-2012>.
- Hoppmann, M, Kuznetsov, I, Fang, Y-C, Rabe, B.** 2022. Mesoscale observations of temperature and salinity in the Arctic Transpolar Drift: A high-resolution dataset from the MOSAiC Distributed Network. *Earth System Science Data* **14**: 4901–4921. DOI: <http://dx.doi.org/10.5194/essd-14-4901-2022>.
- Horner, R, Ackley, SF, Dieckmann, GS, Gulliksen, B, Hoshiai, T, Legendre, L, Melnikov, IA, Reeburgh, WS, Spindler, M, Sullivan, CW.** 1992. Ecology of sea ice biota. *Polar Biology* **12**: 417–427. DOI: <http://dx.doi.org/10.1007/BF00243113>.
- Huang, J, Jaeglé, L.** 2017. Wintertime enhancements of sea salt aerosol in polar regions consistent with a sea ice source from blowing snow. *Atmospheric Chemistry and Physics* **17**: 3699–3712. DOI: <http://dx.doi.org/10.5194/acp-17-3699-2017>.
- Huang, S, Hu, W, Chen, J, Wu, Z, Zhang, D, Fu, P.** 2021. Overview of biological ice nucleating particles in the atmosphere. *Environment International* **146**: 106197. DOI: <http://dx.doi.org/10.1016/j.envint.2020.106197>.
- Huffman, JA, Sinha, B, Garland, RM, Snee-Pollmann, A, Gunthe, SS, Artaxo, P, Martin, ST, Andreae, MO, Pöschl, U.** 2012. Size distributions and temporal variations of biological aerosol particles in the Amazon rainforest characterized by microscopy and real-time UV-APS fluorescence techniques during AMAZE-08. *Atmospheric Chemistry and Physics* **12**: 11997–12019. DOI: <http://dx.doi.org/10.5194/acp-12-11997-2012>.
- Irish, VE, Elizondo, P, Chen, J, Chou, C, Charette, J, Lizotte, M, Ladino, LA, Wilson, TW, Gosselin, M, Murray, BJ, Polishchuk, E, Abbatt, JPD, Miller, LA, Bertram, AK.** 2017. Ice-nucleating particles in Canadian Arctic sea-surface microlayer and bulk seawater. *Atmospheric Chemistry and Physics* **17**: 10583–10595. DOI: <http://dx.doi.org/10.5194/acp-17-10583-2017>.
- Istomina, L.** 2020 Dec. Retrieval of sea ice surface melt using OLCI data onboard sentinel-3. AGU Fall Meeting Abstracts; Washington, DC. C017–C107.
- Jayaweera, K, Flanagan, P.** 1982. Investigations on biogenic ice nuclei in the Arctic atmosphere. *Geophysical Research Letters* **9**: 94–97. DOI: <http://dx.doi.org/10.1029/GL009i001p00094>.
- Jung, J, Miyazaki, Y, Hur, J, Lee, YK, Jeon, MH, Lee, Y, Cho, K-H, Chung, HY, Kim, K, Choi, J-O, Lalande, C, Kim, J-H, Choi, T, Yoon, YJ, Yang, EJ, Kang, S-H.** 2023. Measurement report: Summertime fluorescence characteristics of atmospheric water-soluble organic carbon in the marine boundary layer of the western Arctic Ocean. *Atmospheric Chemistry and Physics* **23**: 4663–4684. DOI: <http://dx.doi.org/10.5194/acp-23-4663-2023>.
- Junge, K, Eicken, H, Deming, JW.** 2004. Bacterial activity at –2 to –20°C in Arctic wintertime sea ice. *Applied and Environmental Microbiology* **70**: 550–557. DOI: <http://dx.doi.org/10.1128/AEM.70.1.550-557.2004>.
- Kanji, ZA, Ladino, LA, Wex, H, Boose, Y, Burkert-Kohn, M, Cziczo, DJ, Krämer, M.** 2017. Overview of ice

- nucleating particles. *Meteorological Monographs* **58**: 1.1–1.33. DOI: <http://dx.doi.org/10.1175/AMSMONOGRAPHSD-16-0006.1>.
- Kanzow, T.** 2020. Master track of POLARSTERN cruise PS122/3 in 1 sec resolution. Alfred Wegener Institute, Helmholtz Centre for Polar and Marine Research, Bremerhaven. DOI: <http://dx.doi.org/10.1594/PANGAEA.924678>.
- Kawana, K, Matsumoto, K, Taketani, F, Miyakawa, T, Kanaya, Y.** 2021. Fluorescent biological aerosol particles over the central Pacific Ocean: Covariation with ocean surface biological activity indicators. *Atmospheric Chemistry and Physics* **21**: 15969–15983. DOI: <http://dx.doi.org/10.5194/acp-21-15969-2021>.
- Kawana, K, Taketani, F, Matsumoto, K, Tobo, Y, Iwamoto, Y, Miyakawa, T, Ito, A, Kanaya, Y.** 2024. Roles of marine biota in the formation of atmospheric bioaerosols, cloud condensation nuclei, and ice-nucleating particles over the North Pacific Ocean, Bering Sea, and Arctic Ocean. *Atmospheric Chemistry and Physics* **24**: 1777–1799. DOI: <http://dx.doi.org/10.5194/acp-24-1777-2024>.
- Kim, Y-H, Min, S-K, Gillett, NP, Notz, D, Malinina, E.** 2023. Observationally-constrained projections of an ice-free Arctic even under a low emission scenario. *Nature Communications* **14**: 3139. DOI: <http://dx.doi.org/10.1038/s41467-023-38511-8>.
- Kirpes, RM, Bonanno, D, May, NW, Fraund, M, Barget, AJ, Moffet, RC, Ault, AP, Pratt, KA.** 2019. Winter-time Arctic Sea spray aerosol composition controlled by sea ice lead microbiology. *ACS Central Science* **5**: 1760–1767. DOI: <http://dx.doi.org/10.1021/acscentsci.9b00541>.
- Knap, AH, Ducklow, H, Michaels, A, Dickson, A** eds. 1996. Protocols for the Joint Global Ocean Flux Study (JGOFS) core measurements (JGOFS Report No. 19, vi+170). PANGAEA.
- Korolev, A, McFarquhar, G, Field, PR, Franklin, C, Lawson, P, Wang, Z, Williams, E, Abel, SJ, Axisa, D, Borrmann, S, Crosier, J, Fugal, J, Krämer, M, Lohmann, U, Schlenczek, O, Schnaiter, M, Wendisch, M.** 2017. Mixed-phase clouds: Progress and challenges. *Meteorological Monographs* **58**(1): 5.1–5.50. DOI: <http://dx.doi.org/10.1175/AMSMONOGRAPHSD-17-0001.1>.
- Kramer, M, Kiko, R.** 2011. Brackish meltponds on Arctic Sea ice—A new habitat for marine metazoans. *Polar Biology* **34**: 603–608. DOI: <http://dx.doi.org/10.1007/s00300-010-0911-z>.
- Kruppen, T, von Albedyll, L, Goessling, HF, Hendricks, S, Juhls, B, Spreen, G, Willmes, S, Belter, HJ, Dethloff, K, Haas, C, Kaleschke, L, Katlein, C, Tian-Kunze, X, Ricker, R, Rostosky, P, Rückert, J, Singha, S, Sokolova, J.** 2021. MOSAiC drift expedition from October 2019 to July 2020: Sea ice conditions from space and comparison with previous years. *The Cryosphere* **15**: 3897–3920. DOI: <http://dx.doi.org/10.5194/tc-15-3897-2021>.
- Leck, C, Bigg, EK.** 1999. Aerosol production over remote marine areas—a new route. *Geophysical Research Letters* **26**: 3577–3580. DOI: <http://dx.doi.org/10.1029/1999GL010807>.
- Leck, C, Bigg, EK.** 2005. Source and evolution of the marine aerosol—a new perspective. *Geophysical Research Letters* **32**(19). DOI: <http://dx.doi.org/10.1029/2005GL023651>.
- Leck, C, Norman, M, Bigg, EK, Hillamo, R.** 2002. Chemical composition and sources of the high Arctic aerosol relevant for cloud formation. *Journal of Geophysical Research: Atmospheres* **107**(D12): AAC 1-1–AAC 1-17. DOI: <http://dx.doi.org/10.1029/2001JD001463>.
- Leck, C, Persson, C.** 1996. The central Arctic Ocean as a source of dimethyl sulfide seasonal variability in relation to biological activity. *Tellus B: Chemical and Physical Meteorology* **48**: 156–177. DOI: <http://dx.doi.org/10.3402/tellusb.v48i2.15834>.
- Li, L, Pomeroy, JW.** 1997. Estimates of threshold wind speeds for snow transport using meteorological data. *Journal of Applied Meteorology and Climatology* **36**: 205–213. DOI: [http://dx.doi.org/10.1175/1520-0450\(1997\)036<0205:EOTWSF>2.0.CO;2](http://dx.doi.org/10.1175/1520-0450(1997)036<0205:EOTWSF>2.0.CO;2).
- Mahmood, R, von Salzen, K, Flanner, M, Sand, M, Langner, J, Wang, H, Huang, L.** 2016. Seasonality of global and Arctic black carbon processes in the Arctic monitoring and assessment programme models: Global and Arctic black carbon processes. *Journal of Geophysical Research: Atmospheres* **121**(12): 7100–7116. DOI: <http://dx.doi.org/10.1002/2016JD024849>.
- Malard, L, Avila-Jimenez, M, Convey, P, Larose, C, Hodson, A, Øvreås, L, Schmale, J, Anwar, M, Pearce, DA.** 2018. Microbial activity monitoring by the integrated Arctic earth observing system (MamSIOS), in Orr, E, Hansen, G, Lappalainen, H, Hübner, C, Lihavainen, H eds., *SESS report 2018*. Longyearbyen, Svalbard: Svalbard Integrated Arctic Earth Observing System (SIOS): 48–81.
- May, NW, Olson, NE, Panas, M, Axson, JL, Tirella, PS, Kirpes, RM, Craig, RL, Gunsch, MJ, China, S, Laskin, A, Ault, AP, Pratt, KA.** 2018. Aerosol emissions from Great Lakes harmful algal blooms. *Environmental Science & Technology* **52**: 397–405. DOI: <http://dx.doi.org/10.1021/acs.est.7b03609>.
- May, NW, Quinn, PK, McNamara, SM, Pratt, KA.** 2016. Multiyear study of the dependence of sea salt aerosol on wind speed and sea ice conditions in the coastal Arctic. *Journal of Geophysical Research: Atmospheres* **121**: 9208–9219. DOI: <http://dx.doi.org/10.1002/2016JD025273>.
- Mirrielees, JA, Kirpes, RM, Haas, SM, Rauschenberg, CD, Matrai, PA, Remenapp, A, Boschi, VL, Granmas, AM, Pratt, KA, Ault, AP.** 2022. Probing individual particles generated at the freshwater–seawater interface through combined Raman, photothermal infrared, and X-ray spectroscopic characterization. *ACS Measurement Science* **2**(6): 605–619. DOI: <http://dx.doi.org/10.1021/acsmesuresci.2c00041>.

- Moallemi, A, Landwehr, S, Robinson, C, Simó, R, Zamani, M, Chen, G, Baccarini, A, Schnaiter, M, Henning, S, Modini, RL, Gysel-Beer, M, Schmale, J.** 2021. Sources, occurrence and characteristics of fluorescent biological aerosol particles measured over the pristine Southern Ocean. *Journal of Geophysical Research: Atmospheres* **126**(11): e2021JD034811. DOI: <http://dx.doi.org/10.1029/2021JD034811>.
- Möhler, O, DeMott, PJ, Vali, G, Levin, Z.** 2007. Microbiology and atmospheric processes: The role of biological particles in cloud physics. *Biogeosciences* **4**(6): 1059–1071. DOI: <http://dx.doi.org/10.5194/bg-4-1059-2007>.
- Morrison, H, de Boer, G, Feingold, G, Harrington, J, Shupe, MD, Sulia, K.** 2012. Resilience of persistent Arctic mixed-phase clouds. *Nature Geoscience* **5**: 11–17. DOI: <http://dx.doi.org/10.1038/ngeo1332>.
- Mostofa, KMG, Liu, C, Yoshioka, T, Vione, D, Zhang, Y, Sakugawa, H.** 2013. Fluorescent dissolved organic matter in natural waters, in Mostofa, KMG, Yoshioka, T, Mottaleb, A, Vione, D eds. *Photobiogeochemistry of organic matter: Principles and practices in water environments, Environmental science and engineering*. Berlin, Heidelberg: Springer: 429–559. DOI: [http://dx.doi.org/10.1007/978-3-642-32223-5\\_6](http://dx.doi.org/10.1007/978-3-642-32223-5_6).
- Müller, O, Fong, AA, Snoeijis-Leijonmalm, P, Creamean, J, Olsen, LM, Eggers, L, Grosse, J, Hoppe, CJM, Torstensson, A, Heitman, L, Balmonte, JP, Chamberlain, E, Dietrich, U, Larsen, A, Petelenz, E, Tsagaraki, TM, Mayers, K, Langvad, M, Granskog, MA, Bratbak, G.** 2023. Flow cytometry dataset from CTD casts showing the abundance of microorganisms (smaller than 20 µm) during the Arctic MOSAiC expedition. PANGAEA. DOI: <http://dx.doi.org/10.1594/PANGAEA.963430>.
- Nicolaus, M, Arndt, S, Birnbaum, G, Katlein, C.** 2021. Visual panoramic photographs of the surface conditions during the MOSAiC campaign 2019/20. PANGAEA. DOI: <http://dx.doi.org/10.1594/PANGAEA.938534>.
- Nicolaus, M, Perovich, DK, Spreen, G, Granskog, MA, von Albedyll, L, Angelopoulos, M, Anhaus, P, Arndt, S, Belter, H, Bessonov, V, Birnbaum, G, Brauchle, J, Calmer, R, Cardellach, E, Cheng, B, Clemens-Sewall, D, Dacic, R, Damm, E, de Boer, G, Demir, O, Dethloff, K, Divine, DV, Fong, AA, Fons, S, Frey, MM, Fuchs, N, Gabarró, C, Gerland, S, Goessling, HF, Gradinger, R, Haapala, J, Haas, C, Hamilton, J, Hannula, H-R, Hendricks, S, Herber, A, Heuzé, C, Hoppmann, M, Høyland, KV, Huntemann, M, Hutchings, JK, Hwang, B, Itkin, P, Jacobi, H-W, Jaggi, M, Jutila, A, Kaleschke, L, Katlein, C, Kolabutin, N, Krampe, D, Kristensen, SS, Krumpfen, T, Kurtz, N, Lampert, A, Lange, BA, Lei, R, Light, B, Linhardt, F, Liston, GE, Loose, B, Macfarlane, AR, Mahmud, M, Matero, IO, Maus, S, Morgenstern, A, Naderpour, R, Nandan, V, Niubom, A, Oggier, M, Oppelt, N, Pätzold, F, Perron, C, Petrovsky, T, Pirazzini, R, Polashenski, C, Rabe, B, Raphael, IA, Regnery, J, Rex, M, Ricker, R, Riemann-Campe, K, Rinke, A, Rohde, J, Salganik, E, Scharien, RK, Schiller, M, Schneebeli, M, Semmling, M, Shimanchuk, E, Shupe, MD, Smith, MM, Smolyanitsky, V, Sokolov, V, Stanton, T, Stroeve, J, Thielke, L, Timofeeva, A, Tonboe, RT, Tavri, A, Tsamados, M, Wagner, DN, Watkins, D, Webster, M, Wendisch, M.** 2022. Overview of the MOSAiC expedition: Snow and sea ice. *Elementa: Science of the Anthropocene* **10**: 000046. DOI: <http://dx.doi.org/10.1525/elementa.2021.000046>.
- Niebauer, HJ.** 1991. Bio-physical oceanographic interactions at the edge of the Arctic ice pack. *Journal of Marine Systems* **2**(1–2): 209–232. DOI: [http://dx.doi.org/10.1016/0924-7963\(91\)90025-P](http://dx.doi.org/10.1016/0924-7963(91)90025-P).
- Nilsson, ED, Rannik, Ü, Swietlicki, E, Leck, C, Aalto, PP, Zhou, J, Norman, M.** 2001. Turbulent aerosol fluxes over the Arctic Ocean: 2. Wind-driven sources from the sea. *Journal of Geophysical Research: Atmospheres* **106**: 32139–32154. DOI: <http://dx.doi.org/10.1029/2000JD900747>.
- Nixdorf, U, Dethloff, K, Rex, M, Shupe, M, Sommerfeld, A, Perovich, DK, Nicolaus, M, Heuzé, C, Rabe, B, Loose, B, Damm, E, Gradinger, R, Fong, A, Maslowski, W, Rinke, A, Kwok, R, Spreen, G, Wendisch, M, Herber, A, Hirsekorn, M, Mohaupt, V, Frickenhaus, S, Immerz, A, Weiss-Tuider, K, König, B, Mergedoh, D, Regnery, J, Gerchow, P, Ransby, D, Krumpfen, T, Morgenstern, A, Haas, C, Kanzow, T, Rack, FR, Saitzev, V, Sokolov, V, Makarov, A, Schwarze, S, Wunderlich, T, Wurr, K, Boetius, A.** 2021. MOSAiC Extended Acknowledgement. Zenodo. DOI: <http://dx.doi.org/10.5281/zenodo.5541624>.
- Norris, SJ, Brooks, IM, de Leeuw, G, Sirevaag, A, Leck, C, Brooks, BJ, Birch, CE, Tjernström, M.** 2011. Measurements of bubble size spectra within leads in the Arctic summer pack ice. *Ocean Science* **7**: 129–139. DOI: <http://dx.doi.org/10.5194/os-7-129-2011>.
- Olsen, LM, Laney, SR, Duarte, P, Kauko, HM, Fernández-Méndez, M, Mundy, CJ, Rösel, A, Meyer, A, Itkin, P, Cohen, L, Peeken, I, Tatarek, A, Róžańska-Pluta, M, Wiktor, J, Taskjelle, T, Pavlov, AK, Hudson, SR, Granskog, MA, Hop, H, Assmy, P.** 2017. The seeding of ice algal blooms in Arctic pack ice: The multiyear ice seed repository hypothesis. *Journal of Geophysical Research: Biogeosciences* **122**: 1529–1548. DOI: <http://dx.doi.org/10.1002/2016JG003668>.
- Orellana, MV, Matrai, PA, Leck, C, Rauschenberg, CD, Lee, AM, Coz, E.** 2011. Marine microgels as a source of cloud condensation nuclei in the high Arctic. *Proceedings of the National Academy of Sciences* **108**: 13612–13617. DOI: <http://dx.doi.org/10.1073/pnas.1102457108>.
- Ovadnevaite, J, Ceburnis, D, Canagaratna, M, Berresheim, H, Bialek, J, Martucci, G, Worsnop, DR, O'Dowd, C.** 2012. On the effect of wind speed on submicron sea salt mass concentrations and source fluxes. *Journal of Geophysical Research: Atmospheres*



- 117(D16). DOI: <http://dx.doi.org/10.1029/2011JD017379>.
- Park, K-T, Lee, K, Kim, T-W, Yoon, YJ, Jang, E-H, Jang, S, Lee, B-Y, Hermansen, O.** 2018. Atmospheric DMS in the Arctic Ocean and its relation to phytoplankton biomass. *Global Biogeochemical Cycles* **32**: 351–359. DOI: <http://dx.doi.org/10.1002/2017GB005805>.
- Patterson, JP, Collins, DB, Michaud, JM, Axson, JL, Sultana, CM, Moser, T, Dommer, AC, Conner, J, Grassian, VH, Stokes, MD, Deane, GB, Evans, JE, Burkart, MD, Prather, KA, Gianneschi, NC.** 2016. Sea spray aerosol structure and composition using cryogenic transmission electron microscopy. *ACS Central Science* **2**: 40–47. DOI: <http://dx.doi.org/10.1021/acscentsci.5b00344>.
- Perrette, M, Yool, A, Quartly, GD, Popova, EE.** 2011. Near-ubiquity of ice-edge blooms in the Arctic. *Biogeosciences* **8**: 515–524. DOI: <http://dx.doi.org/10.5194/bg-8-515-2011>.
- Perring, AE, Mediavilla, B, Wilbanks, GD, Churnside, JH, Marchbanks, R, Lamb, KD, Gao, R-S.** 2023. Airborne bioaerosol observations imply a strong terrestrial source in the summertime Arctic. *Journal of Geophysical Research: Atmospheres* **128**: e2023JD039165. DOI: <http://dx.doi.org/10.1029/2023JD039165>.
- Perring, AE, Schwarz, JP, Baumgardner, D, Hernandez, MT, Spracklen, DV, Heald, CL, Gao, RS, Kok, G, McMeeking, GR, McQuaid, JB, Fahey, DW.** 2015. Airborne observations of regional variation in fluorescent aerosol across the United States. *Journal of Geophysical Research: Atmospheres* **120**: 1153–1170. DOI: <http://dx.doi.org/10.1002/2014JD022495>.
- Pisso, I, Sollum, E, Grythe, H, Kristiansen, NI, Cassiani, M, Eckhardt, S, Arnold, D, Morton, D, Thompson, RL, Groot Zwaftink, CD, Evangeliou, N, Sodemann, H, Haimberger, L, Henne, S, Brunner, D, Burkhardt, JF, Fouilloux, A, Brioude, J, Philipp, A, Seibert, P, Stohl, A.** 2019. The Lagrangian particle dispersion model FLEXPART version 10.4. *Geoscientific Model Development* **12**(12): 4955–4997. DOI: <http://dx.doi.org/10.5194/gmd-12-4955-2019>.
- Pithan, F, Mauritsen, T.** 2014. Arctic amplification dominated by temperature feedbacks in contemporary climate models. *Nature Geoscience* **7**: 181–184. DOI: <http://dx.doi.org/10.1038/ngeo2071>.
- Piwosz, K, Wiktor, JM, Niemi, A, Tatarek, A, Michel, C.** 2013. Mesoscale distribution and functional diversity of picoeukaryotes in the first-year sea ice of the Canadian Arctic. *The ISME Journal* **7**: 1461–1471. DOI: <http://dx.doi.org/10.1038/ismej.2013.39>.
- Pöhlker, C, Huffman, JA, Pöschl, U.** 2012. Autofluorescence of atmospheric bioaerosols—Fluorescent biomolecules and potential interferences. *Atmospheric Measurement Techniques* **5**: 37–71. DOI: <http://dx.doi.org/10.5194/amt-5-37-2012>.
- Pöschl, U, Martin, ST, Sinha, B, Chen, Q, Gunthe, SS, Huffman, JA, Borrmann, S, Farmer, DK, Garland, RM, Helas, G, Jimenez, JL, King, SM, Manzi, A, Mikhailov, E, Pauliquevis, T, Petters, MD, Prenni, AJ, Roldin, P, Rose, D, Schneider, J, Su, H, Zorn, SR, Artaxo, P, Andreae, MO.** 2010. Rainforest aerosols as biogenic nuclei of clouds and precipitation in the Amazon. *Science* **329**: 1513–1516. DOI: <http://dx.doi.org/10.1126/science.1191056>.
- Prather, KA, Bertram, TH, Grassian, VH, Deane, GB, Stokes, MD, DeMott, PJ, Aluwihare, LI, Palenik, BP, Azam, F, Seinfeld, JH, Moffet, RC, Molina, MJ, Cappa, CD, Geiger, FM, Roberts, GC, Russell, LM, Ault, AP, Baltrusaitis, J, Collins, DB, Corrigan, C. E., Cuadra-Rodriguez, L.A., Ebben, C.J., Forestieri, S.D., Guasco, T.L., Hersey, SP, Kim, MJ, Lambert, WF, Modini, RL, Mui, W, Pedler, BE, Ruppel, MJ, Ryder, OS, Schoepp, NG, Sullivan, RC, Zhao, D.** 2013. Bringing the ocean into the laboratory to probe the chemical complexity of sea spray aerosol. *Proceedings of the National Academy of Sciences* **110**: 7550–7555. DOI: <http://dx.doi.org/10.1073/pnas.1300262110>.
- Pratt, KA, DeMott, PJ, French, JR, Wang, Z, Westphal, DL, Heymsfield, AJ, Twohy, CH, Prenni, AJ, Prather, K.A.** 2009. In situ detection of biological particles in cloud ice-crystals. *Nature Geoscience* **2**: 398–401. DOI: <http://dx.doi.org/10.1038/ngeo521>.
- Pusz, W, Urbaniak, J.** 2021. Airborne fungi in Longyearbyen area (Svalbard, Norway)—Case study. *Environmental Monitoring and Assessment* **193**: 290. DOI: <http://dx.doi.org/10.1007/s10661-021-09090-2>.
- Quinn, PK, Collins, DB, Grassian, VH, Prather, KA, Bates, TS.** 2015. Chemistry and related properties of freshly emitted sea spray aerosol. *Chemical Reviews* **115**: 4383–4399. DOI: <http://dx.doi.org/10.1021/cr500713g>.
- Quinn, PK, Shaw, G, Andrews, E, Dutton, EG, Ruoho-Airola, T, Gong, SL.** 2007. Arctic haze: Current trends and knowledge gaps. *Tellus B* **59**: 99–114. DOI: <https://doi.org/10.1111/j.1600-0889.2006.00236.x>.
- Rabe, B, Heuzé, C, Regnery, J, Aksenov, Y, Allerholt, J, Athanase, M, Bai, Y, Basque, C, Bauch, D, Baumann, TM, Chen, D, Cole, ST, Craw, L, Davies, A, Damm, E, Dethloff, K, Divine, DV, Doglioni, F, Ebert, F, Fang, Y-C, Fer, I, Fong, AA, Gradinger, R, Granskog, MA, Graupner, R, Haas, C, He, H, He, Y, Hoppmann, M, Janout, M, Kadko, D, Kanzow, T, Karam, S, Kawaguchi, Y, Koenig, Z, Kong, B, Krishfield, RA, Krumpfen, T, Kuhlmeier, D, Kuznetsov, I, Lan, M, Laukert, G, Lei, R, Li, T, Torres-Valdés, S, Lin, L, Lin, L, Liu, H, Liu, N, Loose, B, Ma, X, McKay, R, Mallet, M, Mallett, RDC, Maslowski, W, Mertens, C, Mohrholz, V, Muilwijk, M, Nicolaus, M, O'Brien, JK, Perovich, D, Ren, J, Rex, M, Ribeiro, N, Rinke, A, Schaffer, J, Schuffenhauer, I, Schulz, K, Shupe, MD, Shaw, W, Sokolov, V, Sommerfeld, A, Spreen, G, Stanton, T, Stephens, M, Su, J, Sukhikh, N, Sundfjord, A, Thomisch, K, Tippenhauer, S, Toole, JM, Vredenburg, M, Walter, M, Wang, H, Wang, L, Wang, Y, Wendisch, M, Zhao, J, Zhou, M, Zhu, J.** 2022. Overview of the MOSAiC expedition: Physical

- oceanography. *Elementa: Science of the Anthropocene* **10**: 00062. DOI: <http://dx.doi.org/10.1525/elementa.2021.00062>.
- Rantanen, M, Karpechko, AY, Lipponen, A, Nordling, K, Hyvärinen, O, Ruosteenoja, K, Vihma, T, Laaksonen, A.** 2022. The Arctic has warmed nearly four times faster than the globe since 1979. *Communications Earth & Environment* **3**: 1–10. DOI: <http://dx.doi.org/10.1038/s43247-022-00498-3>.
- Raven, JA.** 1998. The twelfth Tansley lecture, small is beautiful: The picophytoplankton. *Functional Ecology* **12**: 503–513.
- Reiser, F, Willmes, S, Heinemann, G.** 2020. A new algorithm for daily sea ice lead identification in the Arctic and Antarctic winter from thermal-infrared satellite imagery. *Remote Sensing* **12**: 1957. DOI: <http://dx.doi.org/10.3390/rs12121957>.
- Rex, M.** 2020. Master track of POLARSTERN cruise PS122/1 in 1 sec resolution. Alfred Wegener Institute, Helmholtz Centre for Polar and Marine Research, Bremerhaven. DOI: <http://dx.doi.org/10.1594/PANGAEA.924669>.
- Rex, M.** 2021a. Master track of POLARSTERN cruise PS122/4 in 1 sec resolution. Alfred Wegener Institute, Helmholtz Centre for Polar and Marine Research, Bremerhaven. DOI: <http://dx.doi.org/10.1594/PANGAEA.926830>.
- Rex, M.** 2021b. Master track of POLARSTERN cruise PS122/5 in 1 sec resolution. Alfred Wegener Institute, Helmholtz Centre for Polar and Marine Research, Bremerhaven. DOI: <http://dx.doi.org/10.1594/PANGAEA.926911>.
- Rinke, A, Cassano, JJ, Cassano, EN, Jaiser, R, Handorf, D.** 2021. Meteorological conditions during the MOSAiC expedition. *Elementa: Science of the Anthropocene* **9**: 00023. DOI: <http://dx.doi.org/10.1525/elementa.2021.00023>.
- Salganik, E, Katlein, C, Lange, BA, Matero, I, Lei, R, Fong, AA, Fons, SW, Divine, D, Oggier, M, Castellani, G, Bozzato, D, Chamberlain, EJ, Hoppe, CJM, Müller, O, Gardner, J, Rinke, A, Pereira, PS, Ulfso, A, Marsay, C, Webster, MA, Maus, S, Høyland, KV, Granskog, MA.** 2023. Temporal evolution of under-ice meltwater layers and false bottoms and their impact on summer Arctic Sea ice mass balance. *Elementa: Science of the Anthropocene* **11**: 00035. DOI: <http://dx.doi.org/10.1525/elementa.2022.00035>.
- Sand, M, Berntsen, TK, von Salzen, K, Flanner, MG, Langner, J, Victor, DG.** 2015. Response of Arctic temperature to changes in emissions of short-lived climate forcers. *Nature Climate Change* **6**: 286–289. DOI: <http://dx.doi.org/10.1038/nclimate2880>.
- Santander, MV, Mitts, BA, Pendergraft, MA, Dinasquet, J, Lee, C, Moore, AN, Cancelada, LB, Kimble, KA, Malfatti, F, Prather, KA.** 2021. Tandem fluorescence measurements of organic matter and bacteria released in sea spray aerosols. *Environmental Science & Technology* **55**: 5171–5179. DOI: <http://dx.doi.org/10.1021/acs.est.0c05493>.
- Savage, NJ, Krentz, CE, Könemann, T, Han, TT, Mainelis, G, Pöhlker, C, Huffman, JA.** 2017. Systematic characterization and fluorescence threshold strategies for the wideband integrated bioaerosol sensor (WIBS) using size-resolved biological and interfering particles. *Atmospheric Measurement Techniques* **10**: 4279–4302. DOI: <http://dx.doi.org/10.5194/amt-10-4279-2017>.
- Schmale, J, Schneider, J, Ancellet, G, Quennehen, B, Stohl, A, Sodemann, H, Burkhardt, JF, Hamburger, T, Arnold, SR, Schwarzenboeck, A, Borrmann, S, Law, KS.** 2011. Source identification and airborne chemical characterisation of aerosol pollution from long-range transport over Greenland during POLARCAT summer campaign 2008. *Atmospheric Chemistry and Physics* **11**: 10097–10123. DOI: <http://dx.doi.org/10.5194/acp-11-10097-2011>.
- Schmale, J, Sharma, S, Decesari, S, Pernov, J, Massling, A, Hansson, H-C, von Salzen, K, Skov, H, Andrews, E, Quinn, PK, Upchurch, LM, Eleftheriadis, K, Traversi, R, Gilardoni, S, Mazzola, M, Laing, J, Hopke, P.** 2022. Pan-Arctic seasonal cycles and long-term trends of aerosol properties from 10 observatories. *Atmospheric Chemistry and Physics* **22**: 3067–3096. DOI: <http://dx.doi.org/10.5194/acp-22-3067-2022>.
- Schmale, J, Zieger, P, Ekman, AML.** 2021. Aerosols in current and future Arctic climate. *Nature Climate Change* **11**: 95–105. DOI: <http://dx.doi.org/10.1038/s41558-020-00969-5>.
- Schmithuesen, H.** 2021a. Continuous meteorological surface measurement during POLARSTERN cruise PS122/1. Alfred Wegener Institute, Helmholtz Centre for Polar and Marine Research, Bremerhaven. DOI: <http://dx.doi.org/10.1594/PANGAEA.935221>.
- Schmithuesen, H.** 2021b. Continuous meteorological surface measurement during POLARSTERN cruise PS122/2. Alfred Wegener Institute, Helmholtz Centre for Polar and Marine Research, Bremerhaven. DOI: <http://dx.doi.org/10.1594/PANGAEA.935222>.
- Schmithuesen, H.** 2021c. Continuous meteorological surface measurement during POLARSTERN cruise PS122/3. Alfred Wegener Institute, Helmholtz Centre for Polar and Marine Research, Bremerhaven. DOI: <http://dx.doi.org/10.1594/PANGAEA.935223>.
- Schmithuesen, H.** 2021d. Continuous meteorological surface measurement during POLARSTERN cruise PS122/4. Alfred Wegener Institute, Helmholtz Centre for Polar and Marine Research, Bremerhaven. DOI: <http://dx.doi.org/10.1594/PANGAEA.935224>.
- Schmithuesen, H.** 2021e. Continuous meteorological surface measurement during POLARSTERN cruise PS122/5. Alfred Wegener Institute, Helmholtz Centre for Polar and Marine Research, Bremerhaven. DOI: <http://dx.doi.org/10.1594/PANGAEA.935225>.
- Schneider, J, Höhler, K, Heikkilä, P, Keskinen, J, Bertozzi, B, Bogert, P, Schorr, T, Umo, NS, Vogel, F, Brasseur, Z, Wu, Y, Hakala, S, Duplissy, J, Moiseev, D, Kulmala, M, Adams, MP, Murray, BJ, Korhonen, K, Hao, L, Thomson, ES, Castarède, D,**

- Leisner, T, Petäjä, T, Möhler, O. 2021. The seasonal cycle of ice-nucleating particles linked to the abundance of biogenic aerosol in boreal forests. *Atmospheric Chemistry and Physics* **21**: 3899–3918. DOI: <https://doi.org/10.5194/acp-21-3899-2021>.
- Schulz, K, Koenig, Z, Mulwijk, M, Bauch, D, Hoppe, CJM, Droste, E, Hoppmann, M, Chamberlain, EJ, Laukert, G, Stanton, T, Zurita, AQ, Fer, I, Heuzé, C, Karam, S, Mieruch-Schnuelle, S, Baumann, T, Vredenburg, M, Tippenhauer, S, Granskog, MA. 2023. The Eurasian Arctic Ocean along the MOSAiC drift (2019–2020): An interdisciplinary perspective on properties and processes (version 2). *EarthArXiv* preprints.
- Scott, WD, Levin, Z. 1972. Open channels in sea ice (leads) as ion sources. *Science* **177**: 425–426. DOI: <http://dx.doi.org/10.1126/science.177.4047.425>.
- Serreze, MC, Barry, RG. 2011. Processes and impacts of Arctic amplification: A research synthesis. *Global and Planetary Change* **77**: 85–96. DOI: <http://dx.doi.org/10.1016/j.gloplacha.2011.03.004>.
- Shupe, MD, Intrieri, JM. 2004. Cloud radiative forcing of the arctic surface: The influence of cloud properties, surface albedo, and solar zenith angle. *Journal of Climate* **17**: 13.
- Shupe, MD, Rex, M, Blomquist, B, Persson, POG, Schmale, J, Uttal, T, Althausen, D, Angot, H, Archer, S, Bariteau, L, Beck, I, Bilberry, J, Bucci, S, Buck, C, Boyer, M, Brasseur, Z, Brooks, IM, Calmer, R, Cassano, J, Castro, V, Chu, D, Costa, D, Cox, CJ, Creamean, J, Crewell, S, Dahlke, S, Damm, E, de Boer, G, Deckelmann, H, Dethloff, K, Dütsch, M, Ebell, K, Ehrlich, A, Ellis, J, Engelmann, R, Fong, AA, Frey, MM, Gallagher, MR, Ganzeveld, L, Gradinger, R, Graeser, J, Greenamyre, V, Griesche, H, Griffiths, S, Hamilton, J, Heinemann, G, Helmig, D, Herber, A, Heuzé, C, Hofer, J, Houchens, T, Howard, D, Inoue, J, Jacobi, H-W, Jaiser, R, Jokinen, T, Jourdan, O, Jozef, G, King, W, Kirchgaessner, A, Klingebiel, M, Krassovski, M, Krumpfen, T, Lampert, A, Landing, W, Laurila, T, Lawrence, D, Lonardi, M, Loose, B, Lüpkes, C, Maahn, M, Macke, A, Maslowski, W, Marsay, C, Maturilli, M, Mech, M, Morris, S, Moser, M, Nicolaus, M, Ortega, P, Osborn, J, Pätzold, F, Perovich, DK, Petäjä, T, Pilz, C, Pirazzini, R, Posman, K, Powers, H, Pratt, KA, Preußner, A, Quéléver, L, Radenz, M, Rabe, B, Rinke, A, Sachs, T, Schulz, A, Siebert, H, Silva, T, Solomon, A, Sommerfeld, A, Spreen, G, Stephens, M, Stohl, A, Svensson, G, Uin, J, Viegas, J, Voigt, C, von der Gathen, P, Wehner, B, Welker, JM, Wendisch, M, Werner, M, Xie, Z, Yue, F. 2022. Overview of the MOSAiC expedition: Atmosphere. *Elementa: Science of the Anthropocene* **10**: 00060. DOI: <http://dx.doi.org/10.1525/elementa.2021.00060>.
- Smith, MM, Angot, H, Chamberlain, EJ, Droste, ES, Karam, S, Mulwijk, M, Webb, AL, Archer, SD, Beck, I, Blomquist, BW, Bowman, J, Boyer, M, Bozzato, D, Chierici, M, Creamean, J, D'Angelo, A, Delille, B, Fer, I, Fong, AA, Fransson, A, Fuchs, N, Gardner, J, Granskog, MA, Hoppe, CJM, Hoppema, M, Hoppmann, M, Mock, T, Muller, S, Müller, O, Nicolaus, M, Nomura, D, Petäjä, T, Salganik, E, Schmale, J, Schmidt, K, Schulz, KM, Shupe, MD, Stefels, J, Thielke, L, Tippenhauer, S, Ulfso, A, van Leeuwe, M, Webster, M, Yoshimura, M, Zhan, L. 2023. Thin and transient meltwater layers and false bottoms in the Arctic Sea ice pack—Recent insights on these historically overlooked features. *Elementa: Science of the Anthropocene* **11**: 00025. DOI: <http://dx.doi.org/10.1525/elementa.2023.00025>.
- Solomon, A, de Boer, G, Creamean, JM, McComiskey, A, Shupe, MD, Maahn, M, Cox, C. 2018. The relative impact of cloud condensation nuclei and ice nucleating particle concentrations on phase partitioning in Arctic mixed-phase stratocumulus clouds. *Atmospheric Chemistry and Physics* **18**: 17047–17059. DOI: <http://dx.doi.org/10.5194/acp-18-17047-2018>.
- Song, C, Dall'Osto, M, Lupi, A, Mazzola, M, Traversi, R, Becagli, S, Gilardoni, S, Vratolis, S, Yttri, KE, Beddows, DCS, Schmale, J, Brean, J, Kramawijaya, AG, Harrison, RM, Shi, Z. 2021. Differentiation of coarse-mode anthropogenic, marine and dust particles in the High Arctic islands of Svalbard. *Atmospheric Chemistry and Physics* **21**(14): 11317–11335. DOI: <http://dx.doi.org/10.5194/acp-21-11317-2021>.
- Sørensen, HL, Thamdrup, B, Jeppesen, E, Rysgaard, S, Glud, RN. 2017. Nutrient availability limits biological production in Arctic Sea ice melt ponds. *Polar Biology* **40**: 1593–1606. DOI: <http://dx.doi.org/10.1007/s00300-017-2082-7>.
- Sotiropoulou, G, Bossioli, E, Tombrou, M. 2019. Modeling extreme warm-air advection in the Arctic: The role of microphysical treatment of cloud droplet concentration. *Journal of Geophysical Research: Atmospheres* **124**: 3492–3519. DOI: <http://dx.doi.org/10.1029/2018JD029252>.
- Stohl, A. 2006. Characteristics of atmospheric transport into the Arctic troposphere. *Journal of Geophysical Research: Atmospheres* **111**(D11). DOI: <http://dx.doi.org/10.1029/2005JD006888>.
- Stohl, A, Klimont, Z, Eckhardt, S, Kupiainen, K, Shevchenko, VP, Kopeikin, VM, Novigatsky, AN. 2013. Black carbon in the Arctic: The underestimated role of gas flaring and residential combustion emissions. *Atmospheric Chemistry and Physics* **13**: 8833–8855. DOI: <http://dx.doi.org/10.5194/acp-13-8833-2013>.
- Szopa, S, Naik, V, Adhikary, B, Artaxo, P, Berntsen, T, Collins, WD, Fuzzi, S, Gallardo, L, Kiendler-Scharr, A, Klimont, Z, Liao, H, Unger, N, Zanis, P. 2021. Short-lived climate forcers, in Masson-Delmotte, V, Zhai, P, Pirani, A, Connors, SL, Péan, C, Berger, S, Caud, N, Chen, Y, Goldfarb, L, Gomis, MI, Huang, M, Leitzell, K, Lonnoy, E, Matthews, JBR, Maycock, TK, Waterfield, T, Yelekçi, O, Yu, R, Zhou, B eds., *Climate change 2021: The physical science basis. Contribution of Working*

- Group I to the Sixth Assessment Report of the Intergovernmental Panel on Climate Change. Cambridge, UK; New York: Cambridge University Press: 817–922. DOI: <http://dx.doi.org/10.1017/9781009157896.008>.
- Taketani, F, Miyakawa, T, Takigawa, M, Yamaguchi, M, Komazaki, Y, Mordovskoi, P, Takashima, H, Zhu, C, Nishino, S, Tohjima, Y, Kanaya, Y.** 2022. Characteristics of atmospheric black carbon and other aerosol particles over the Arctic Ocean in early autumn 2016: Influence from biomass burning as assessed with observed microphysical properties and model simulations. *Science of the Total Environment* **848**: 157671. DOI: <http://dx.doi.org/10.1016/j.scitotenv.2022.157671>.
- Tatzelt, C, Henning, S, Tummon, F, Hartmann, M, Baccharini, A, Welti, A, Lehtipalo, K, Schmale, J.** 2020. Ice Nucleating Particle number concentration from low-volume sampling over the Southern Ocean during the austral summer of 2016/2017 on board the Antarctic Circumnavigation Expedition (ACE). (1.1) [data set]. DOI: <https://doi.org/10.5281/zenodo.4311665>.
- Terhaar, J, Lauerwald, R, Regnier, P, Gruber, N, Bopp, L.** 2021. Around one third of current Arctic Ocean primary production sustained by rivers and coastal erosion. *Nature Communications* **12**: 169. DOI: <http://dx.doi.org/10.1038/s41467-020-20470-z>.
- Thiele, S, Storesund, JE, Fernández-Méndez, M, Assmy, P, Øvreås, L.** 2022. A winter-to-summer transition of bacterial and archaeal communities in Arctic Sea ice. *Microorganisms* **10**: 1618. DOI: <http://dx.doi.org/10.3390/microorganisms10081618>.
- Torstensson, A, Showalter, GM, Margolin, AR, Shadwick, EH, Deming, JW, Smith, WO Jr.** 2023. Chemical and biological vertical distributions within central Arctic (>82°N) sea ice during late summer. *Marine Ecology Progress Series* **703**: 17–30. DOI: <http://dx.doi.org/10.3354/meps14213>.
- Twomey, S.** 1991. Aerosols, clouds and radiation. *Atmospheric Environment. Part A. General Topics* **25**: 2435–2442. DOI: [http://dx.doi.org/10.1016/0960-1686\(91\)90159-5](http://dx.doi.org/10.1016/0960-1686(91)90159-5).
- Uin, J, Aiken, AC, Dubey, MK, Kuang, C, Pekour, M, Salwen, C, Sedlacek, AJ, Senum, G, Smith, S, Wang, J, Watson, TB, Springston, SR.** 2019. Atmospheric Radiation Measurement (ARM) Aerosol Observing Systems (AOS) for surface-based in situ atmospheric aerosol and trace gas measurements. *Journal of Atmospheric and Oceanic Technology* **36**(12): 2429–2447. DOI: <https://doi.org/10.1175/JTECH-D-19-0077.1>.
- Vader, A, Marquardt, M, Meshram, AR, Gabrielsen, TM.** 2015. Key Arctic phototrophs are widespread in the polar night. *Polar Biology* **38**: 13–21. DOI: <http://dx.doi.org/10.1007/s00300-014-1570-2>.
- Vali, G.** 1971. Quantitative evaluation of experimental results on the heterogeneous freezing nucleation of supercooled liquids. *Journal of the Atmospheric Sciences* **28**: 402–409. DOI: [1175/1520-0469\(1971\)028<0402:QEOERA>2.0.CO;2](http://dx.doi.org/10.1175/1520-0469(1971)028<0402:QEOERA>2.0.CO;2).
- Wassmann, P, Reigstad, M.** 2011. Future Arctic Ocean seasonal ice zones and implications for pelagic-benthic coupling. *Oceanography* **24**: 220–231. DOI: <http://dx.doi.org/10.5670/oceanog.2011.74>.
- Webster, MA, Holland, M, Wright, NC, Hendricks, S, Hutter, N, Itkin, P, Light, B, Linhardt, F, Perovich, DK, Raphael, IA, Smith, MM, von Albedyll, L, Zhang, J.** 2022. Spatiotemporal evolution of melt ponds on Arctic Sea ice: MOSAiC observations and model results. *Elementa: Science of the Anthropocene* **10**: 000072. DOI: <http://dx.doi.org/10.1525/elementa.2021.000072>.
- Wendisch, M, Macke, A, Ehrlich, A, Lüpkes, C, Mech, M, Chechin, D, Dethloff, K, Velasco, CB, Bozem, H, Brückner, M, Clemen, H-C, Crewell, S, Donth, T, Dupuy, R, Ebell, K, Egerer, U, Engelmann, R, Engler, C, Eppers, O, Gehrman, M, Gong, X, Gottschalk, M, Gourbeyre, C, Griesche, H, Hartmann, J, Hartmann, M, Heinold, B, Herber, A, Herrmann, H, Heygster, G, Hoor, P, Jafarisera-jehlou, S, Jäkel, E, Järvinen, E, Jourdan, O, Kästner, U, Kecorius, S, Knudsen, EM, Köllner, F, Kretzschmar, J, Lelli, L, Leroy, D, Maturilli, M, Mei, L, Mertes, S, Mioche, G, Neuber, R, Nicolaus, M, Nomokonova, T, Notholt, J, Palm, M, van Pinxteren, M, Quaas, J, Richter, P, Ruiz-Donoso, E, Schäfer, M, Schmieder, K, Schnaiter, M, Schneider, J, Schwarzenböck, A, Seifert, P, Shupe, MD, Siebert, H, Spreen, G, Stapf, J, Stratmann, F, Vogl, T, Welti, A, Wex, H, Wiedensohler, A, Zanatta, M, Zeppenfeld, S.** 2019. The Arctic cloud puzzle: Using ALOUD/PASCAL multiplatform observations to unravel the role of clouds and aerosol particles in Arctic amplification. *Bulletin of the American Meteorological Society* **100**: 841–871. DOI: <http://dx.doi.org/10.1175/BAMS-D-18-0072.1>.
- Wéry, N, Galès, A, Brunet, Y.** 2017. Bioaerosol sources, in Delort, A-M, Amato, P eds., *Microbiology of aerosols*. Hoboken, NJ: Wiley: 115–135. DOI: <http://dx.doi.org/10.1002/9781119132318.ch2a>.
- Willis, MD, Leaitch, WR, Abbatt, JPD.** 2018. Processes controlling the composition and abundance of Arctic aerosol. *Reviews of Geophysics* **56**: 621–671. DOI: <http://dx.doi.org/10.1029/2018RG000602>.
- Willmes, S, Heinemann, G, Reiser, F.** 2023. ArcLeads: Daily sea-ice lead maps for the Arctic, 2002–2021, NOV–APR. PANGAEA. DOI: <http://dx.doi.org/10.1594/PANGAEA.955561>.
- Winiger, P, Barrett, TE, Sheesley, RJ, Huang, L, Sharma, S, Barrie, LA, Yttri, KE, Evangelidou, N, Eckhardt, S, Stohl, A, Klimont, Z, Heyes, C, Semiletov, IP, Dudarev, OV, Charkin, A, Shakhova, N, Holmstrand, H, Andersson, A, Gustafsson, Ö.** 2019. Source apportionment of circum-Arctic atmospheric black carbon from isotopes and modeling. *Science Advances* **5**: eaau8052. DOI: <http://dx.doi.org/10.1126/sciadv.aau8052>.

- World Meteorological Organization, Global Atmosphere Watch.** 2016. WMO/GAW Aerosol measurement procedures: Guidelines and recommendations. GAW Report No. 227. Geneva, Switzerland: WMO/GAW.
- Yue, S, Li, L, Xu, W, Zhao, J, Ren, H, Ji, D, Li, P, Zhang, Q, Wei, L, Xie, Q, Pan, X, Wang, Z, Sun, Y, Fu, P.** 2022. Biological and nonbiological sources of fluorescent aerosol particles in the urban atmosphere. *Environmental Science & Technology* **56**(12): 7588–7597. DOI: <http://dx.doi.org/10.1021/acs.est.1c07966>.
- Zinke, J, Nilsson, ED, Zieger, P, Salter, ME.** 2022. The effect of seawater salinity and seawater temperature on sea salt aerosol production. *Journal of Geophysical Research: Atmospheres* **127**(16): e2021JD036005. DOI: <http://dx.doi.org/10.1029/2021JD036005>.

**How to cite this article:** Beck, I, Moallemi, A, Heutte, B, Pernov, JB, Bergner, N, Rolo, M, Quéléver, LLJ, Laurila, T, Boyer, M, Jokinen, T, Angot, H, Hoppe, CLM, Müller, O, Creamean, J, Frey, MM, Freitas, G, Zinke, J, Salter, M, Zieger, P, Mirrielees, JA, Kempf, HE, Ault, AP, Pratt, KA, Gysel-Beer, M, Henning, S, Tatzelt, C, Schmale, J. 2024. Characteristics and sources of fluorescent aerosols in the central Arctic Ocean. *Elementa: Science of the Anthropocene* 12(1). DOI: <https://doi.org/10.1525/elementa.2023.00125>

**Domain Editor-in-Chief:** Detlev Helmig, Boulder AIR LLC, Boulder, CO, USA

**Knowledge Domain:** Atmospheric Science

**Part of an Elementa Special Feature:** The Multidisciplinary Drifting Observatory for the Study of Arctic Climate (MOSAIC)

**Published:** May 30, 2024    **Accepted:** April 12, 2024    **Submitted:** October 16, 2023

**Copyright:** © 2024 The Author(s). This is an open-access article distributed under the terms of the Creative Commons Attribution 4.0 International License (CC-BY 4.0), which permits unrestricted use, distribution, and reproduction in any medium, provided the original author and source are credited. See <http://creativecommons.org/licenses/by/4.0/>.